

# CATALYSIS BY GOLD FOR BIOMASS TRANSFORMATIONS



**OLGA A. SIMAKOVA**

ÅBO AKADEMI  
TURKU/ÅBO  
2012





Olga Andreevna Simakova

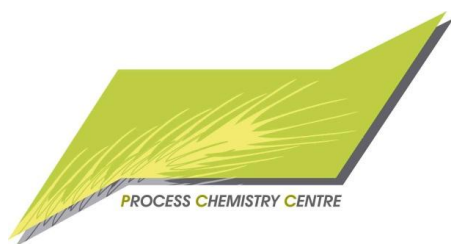
b. 1986 in Novosibirsk, Russia

M. Sc. Chemistry, 2008

Novosibirsk State University, Russia

# Catalysis by gold for biomass transformations

**Olga A. Simakova**



Laboratory of Industrial Chemistry and Reaction Engineering  
Process Chemistry Centre  
Department of Chemical Engineering  
Åbo Akademi University  
Åbo 2012

*Supervised by*

Professor Dmitry Yu. Murzin  
Laboratory of Industrial Chemistry and Reaction Engineering  
Process Chemistry Centre  
Department of Chemical Engineering  
Åbo Akademi University  
Finland

*Reviewers*

Professor Chris Hardacre  
School of Chemistry and Chemical Engineering  
Queen's University of Belfast  
Belfast, Northern Ireland  
United Kingdom

Dr. Catherine Pinel  
Centre National de la Recherche Scientifique  
L'Institut de Recherches sur la Catalyse et l'Environnement de Lyon  
Villeurbanne  
France

*Opponent*

Professor Chris Hardacre  
School of Chemistry & Chemical Engineering  
Queen's University of Belfast  
Belfast, Northern Ireland  
United Kingdom

ISBN 978-952-12-2793-6  
Painosalama Oy – Turku, Finland 2012

## Preface

---

This work was performed between 2008 and 2012 at the Laboratory of Industrial Chemistry and Reaction Engineering, Process Chemistry Centre, Department of Chemical Engineering at Åbo Akademi University. The research is a part of the activities performed at Åbo Akademi Process Chemistry Centre within the Finnish Centre of Excellence Programme (2000-2011).

At this time four years after I started my doctoral studies it is finally time to acknowledge all the people and organizations that in some way or another contribute to this dissertation.

The financial support from Academy of Finland, Graduate School of Materials Research (GSMR) and Graduate School of Chemical Engineering (GSCE) is gratefully acknowledged.

I would like to express my gratitude to Professor Dmitry Yu. Murzin and Academy Professor Tapio Salmi for the opportunity to work at the Laboratory, and conduct research in the fascinating area of catalysis by gold. I sincerely thank you for bringing the inspiration, and for sharing your knowledge and experience with me. I am deeply grateful for your willingness to help not only on my professional development, but also on the personal level. It was an honor to be mentored by you.

I am very grateful to Docent Päivi Mäki-Arvela for the scientific advice and unreserved support from the early stages of my research at Åbo Akademi University; Dr. Kari Eränen for the invaluable help with the reactor systems and very efficient work; Professor Johan Wärnå for the expertise in kinetic modeling. Also, I would like to thank Docent Narendra Kumar for the guidance in the chemistry of zeolites and mesoporous materials. Professor Stefan Willför and Professor Patrik Eklund are gratefully acknowledged for the fruitful scientific input and introduction to the chemistry of wood biomass. Special appreciation goes to Mrs. Elena V. Murzina for her devoted assistance and support in achieving important scientific results.

I would like to thank all the co-authors and co-workers from Åbo Akademi University (Finland), University of Oulu (Finland), University of Helsinki (Finland), Centro de Nanociencias y Nanotecnología at Universidad Nacional Autónoma de México (Mexico), Boreskov Institute of Catalysis (Russia), University of Limerick (Ireland), Université de Strasbourg (France), and University of Virginia (USA) for their contribution to the successful collaboration.

I feel very lucky to be surrounded by good friends. I deeply appreciate their care and their thrust in me. I would like to thank all my friends from Novosibirsk for their support and encouragement, particularly Marina Chubova, Antonina Fedorova, Anna Skovpina, Anastasia Tarasova, and Anna Barsukova. Furthermore, my deep appreciation to my friends and colleagues, Ekaterina Korotkova, Alexey Kirilin, Dr. Anton Tokarev, Dr. Elena Tokareva, Dr. Viktor Vorobyev, Bartosz Rozmyslowicz, Pasi Tolvanen, Cesar Araujo, Gerson Martin, Dr. Bright Kusema, Denys Mavrynsky, Yury Brusentsev, Zhanna Boeva, and researchers from the Laboratory of Industrial Chemistry and Reaction Engineering, who made my life in Finland delightful. These four years were full of adventures and challenges. I really enjoyed your company and all the activities we organized.

Finally, I would like to express my deepest appreciation to my family, particularly to my parents, Andrey and Irina, my brother Valeriy and his wife Daria, grandparents, aunt and uncle, Alexey and Tatyana, for being there for me. Thank you for the understanding, support and encouragement. *Спасибо, что вы у меня есть! Спасибо за то, что вы всегда рядом в трудную минуту и всегда находите нужные слова поддержки.* Moreover, I would like to thank my parents, who are both chemists, for never forcing me to study chemistry, while making me curious about natural sciences. Thank you for your contribution to my personality and of course for your scientific input.

Last but not least, I would like to thank Ernie for his infinite patience and love. Your belief in me and caring is invaluable.

Olga A. Simakova  
Åbo, September 2012

## Abstract

---

Olga A. Simakova

### Catalysis by gold for biomass transformations

Doctoral Thesis, Laboratory of Industrial Chemistry and Reaction Engineering, Process Chemistry Centre, Department of Chemical Engineering, Åbo Akademi University, 2012.

**Keywords:** gold catalysts, linoleic acid, arabinose, ethanol, lignans, hydroxymatairesinol, oxomatairesinol, isomerization, selective oxidation, kinetics, reaction mechanism.

The development of new technologies to supplement fossil resources has led to a growing interest in the utilization of alternative routes. Biomass is a rich renewable feedstock for producing fine chemicals, polymers, and a variety of commodities replacing petroleum-derived chemicals. Transformation of biomass into diverse valuable chemicals is the key concept of a biorefinery. Catalytic conversion of biomass, which reduces the use of toxic chemicals is one of the important approaches to improve the profitability of biorefineries. Utilization of gold catalysts allows conducting reactions under environmentally-friendly conditions, with a high catalytic activity and selectivity. Gold-catalyzed valorization of several biomass-derived compounds as an alternative approach to the existing technologies was studied in this work.

Isomerization of linoleic acid via double bond migration towards biologically active conjugated linoleic acid isomers (CLA) was investigated. The activity and selectivity of various gold catalysts towards *cis*-9,*trans*-11-CLA and *trans*-10,*cis*-12-CLA were investigated in a semi-batch reactor, showing that the yield of the desired products varied, depending on the catalyst support.

The structure sensitivity in the selective oxidation of arabinose was demonstrated using a series of gold catalysts with different Au cluster sizes in a shaker reactor operating in a semi-batch mode. The gas-phase selective oxidation of ethanol was studied and the influence of the catalyst support on the catalytic performance was investigated.

The selective oxidation of the lignan hydroxymatairesinol (HMR), extracted from the Norway spruce (*Picea abies*) knots, to the lignan oxomatairesinol (oxoMAT) was extensively investigated. The influence of the reaction conditions and catalyst properties on the yield of oxoMAT was evaluated. In particular, the structure sensitivity of the reaction was demonstrated. The catalyst deactivation and regeneration procedures were studied. The reaction kinetics and mechanism were advanced.

## Referat

---

Olga A. Simakova

### **Guldkatalyserad omvandling av komponenter i biomassa**

Doktorsavhandling, Laboratoriet för teknisk kemi och reaktionsteknik, Processkemiska centret, Institutionen för kemiteknik, Åbo Akademi 2012

*Nyckelord:* guldkatalysator, linolsyra, arabinos, etanol, lignan, hydroximatairesinol, oxomatairesinol, isomerisering, selektiv oxidation, kinetik, reaktionsmekanism

Utveckling av nya teknologier för att ersätta fossila naturresurser har ökat intresset för alternativa kemiska reaktionsvägar, som baserar sig på utnyttjandet av heterogena katalysatorer, vilkas uppgift är att påskynda kemiska reaktioners hastigheter. Biomassa är en mångsidig förnybar råvara för bas- och finkemikalier samt polymerer, som i framtiden kunde ersätta råoljebaserade kemiska produkter. Omvandling av biomassan till värdefulla kemikalier utgör nyckelkonceptet för ett effektivt bioraffinaderi. Katalytisk omvandling av biomassa, vilket minskar på användningen av giftiga och skadliga kemikalier, är en central faktor vid utvecklingen av lönsamma bioraffinaderier.

Guld, som länge ansågs vara en inaktiv metall i alla katalytiska omvandlingar, har visat sig vara en effektiv heterogen katalysator för många isomeriserings- och oxidationsreaktioner. Användningen av guldkatalysatorer i form av nanopartiklar på porösa bärmaterial gör det möjligt att genomföra kemiska reaktioner under miljövänliga betingelser, så att en hög katalytisk aktivitet och en utmärkt produktselektivitet uppnås. I detta arbete studerades en alternativ teknologi, nämligen guldkatalyserad uppgradering av flera intressanta komponenter, som förekommer i biomassan.

Isomerisering av linolsyra via migrering av dubbelbindningar till biologiskt aktiva linolsyraisomerer (CLA) undersöktes experimentellt i laboratorieskala. Aktiviteten och selektiviteten av olika guldkatalysatorer till önskade produkter studerades i en halvkontinuerlig reaktor. Utbytet av önskade produkter varierade, beroende på katalysatorns bärmaterial.

Strukturkänsligheten för selektiv oxidation av en sockerart, arabinos, till arabinonsyra demonstrerades med en serie av guldkatalysatorer, som hade olika nanoklusterstorlekar. En halvkontinuerlig skakande reaktor användes i experimenten. Selektiv oxidation av etanol studerades också och katalysatorbärmaterialets inverkan på katalysatorns prestanda undersöktes.

En hälsobefrämjande lignankomponent, hydroximatairesinol (HMR) förekommer rikligt i granvedens kvistnötter. Selektiv oxidation av hydroximatairesinol till oxomatairesinol undersöktes ingående i arbetet. Både katalysatorns deaktivering och katalysatorregenerering studerades och reaktionens strukturkänslighet demonstrerades. En reaktionsmekanism föreslogs och en matematisk modell för reaktionens hastighet utvecklades.



## Реферат

---

Ольга Андреевна Симакова

### Превращение компонентов биомассы на золотых катализаторах

Диссертация, Laboratory of Industrial Chemistry and Reaction Engineering, Process Chemistry Centre, Department of Chemical Engineering, Åbo Akademi University, 2012.

*Ключевые слова:* золотые катализаторы, линолевая кислота, арабиноза, этанол, лигнаны, гидроксиматарезинол, оксоматарезинол, изомеризация, селективное окисление, кинетика, механизм реакции.

Развитие новых технологий, дополняющих нефтехимический синтез, вызвало растущий интерес к использованию альтернативных путей. Биомасса – ценное возобновляемое химическое сырье для производства продуктов тонкой химии, полимеров и разнообразных соединений способных заменить продукты, получаемые на основе нефтехимического синтеза. Превращение биомассы в разнообразные ценные химические соединения представляет собой основную концепцию так называемого биоНПЗ. Каталитические превращения биомассы, снижающие использование токсичных химических соединений, являются одним из важнейших методов повышения эффективности биоНПЗ. Использование золотых катализаторов позволяет проводить реакции в условиях благоприятных для окружающей среды при высокой каталитической активности и селективности. В данной работе были изучены реакции превращения компонентов биомассы на золотых катализаторах в ценные химические соединения в качестве альтернативы к уже существующим технологиям.

Была изучена изомеризация линолевой кислоты для получения биологически активных изомеров конъюгированной линолевой кислоты (КЛК). Активность и селективность золотых катализаторов в синтезе *цис*-9,*транс*-11-КЛК и *транс*-10,*цис*-12-КЛК были изучены в реакторе полупроточного типа. Было показано, что выход целевого продукта меняется в зависимости от носителя катализатора.

Структурная чувствительность реакции селективного окисления арабинозы была изучена с использованием золотых катализаторов с различным размером нанесенных золотых частиц в качающемся реакторе в полупроточном режиме.

Было изучено влияние носителя катализатора на каталитическую активность в реакции газофазного селективного окисления этанола.

Наиболее детально была исследована реакция селективного окисления лигнана гидроксиматарезинола (ГМР), экстрагированного из древесной биомассы ели обыкновенной (*Picea abies*), с целью получения лигнана оксоматарезинола (оксоМАТ). Было установлено влияние условий реакции и физико-химических свойств катализатора на выход продукта реакции. Кроме того, была продемонстрирована структурная чувствительность реакции. Были изучены дезактивация и методология регенерации катализатора. В ходе исследования были предложены кинетическая модель и механизм реакции.

## List of Publications

---

- I. **O. A. Simakova**, B. Campo, D. Yu. Murzin, *Gold on carbon catalysts, in Gold nanoparticles: Preparation, characterization and fabrication*, Chapter 5, Nova Science Publishers, Inc. NY, 2010, 147-171.
- II. **O. A. Simakova**, R. J. Davis, D. Yu. Murzin, Biomass processing over gold catalysts, SpringerBriefs in Molecular Science, 2012 (*submitted*).
- III. **O. A. Simakova**, A.-R. Leino, B. Campo, P. Mäki-Arvela, K. Kordás, J.-P. Mikkola, D. Yu. Murzin, *Linoleic acid isomerization over meoporous carbon supported gold catalysts*. Catal. Today, 2010, 150, 32-36.
- IV. **O. A. Simakova**, V. I. Sobolev, K. Yu. Koltunov, B. Campo, A.-R. Leino, K. Kordás, D. Yu. Murzin. *A 'double peak' catalytic activity of nano-sized gold supported on titania in the gas-phase selective oxidation of ethanol*. ChemCatChem, 2010, 2, 1535 – 1538.
- V. V. I. Sobolev, **O. A. Simakova**, K. Yu. Koltunov, *Generation of reactive oxygen species on Au/TiO<sub>2</sub> after treatment with hydrogen: testing the link to ethanol low-temperature oxidation*. ChemCatChem, 2011, 3(9), 1422-1425.
- VI. V. I. Sobolev, K. Yu. Koltunov, **O. A. Simakova**, A.-R. Leino, D. Yu. Murzin, *Low temperature gas-phase oxidation of ethanol over Au/TiO<sub>2</sub>*. Appl. Catal. A, 2012, 433-434, 88-95.
- VII. **O. A. Simakova**, B. T. Kusema, B. C. Campo, A.-R. Leino, K. Kordás, V. Pitchon, P. Mäki-Arvela, D. Yu. Murzin. *Structure sensitivity in L-arabinose oxidation over Au/Al<sub>2</sub>O<sub>3</sub>*. J. Phys. Chem. C., 2011, 115, 1036–1043.
- VIII. **O. A. Simakova**, E. V. Murzina, P. Mäki-Arvela, A.-R. Leino, B. C. Campo, K. Kordás, S. Willför, T. Salmi, D. Yu. Murzin, *Oxidative dehydrogenation of a biomass derived lignan – hydroxymatairesinol over heterogeneous gold catalysts*. J. Catal., 2011, 282, 54-64.
- IX. **O. A. Simakova**, E. Smolentseva, M. Estrada, E. V. Murzina, S. Beloshapkin, S. M. Willför, A. V. Simakov, D. Yu. Murzin, *From woody biomass extractives to health promoting substances: Selective oxidation of the lignan hydroxymatairesinol to oxomatairesinol over Au, Pd and Au-Pd heterogeneous catalysts*, J. Catal., 2012, 291, 95-103.
- X. **O. A. Simakova**, E. V. Murzina, A.-R. Leino, P. Mäki-Arvela, S. M. Willför, D. Yu. Murzin, *Gold catalysts for selective aerobic oxidation of the lignan hydroxymatairesinol to oxomatairesinol: catalyst deactivation and regeneration*, Catal. Lett., 2012, 142, 1011-1019.
- XI. A. Prestianni, F. Ferrante, **O. Simakova**, D. Duca, D. Yu. Murzin, *Secondary-Alcohol Oxidation over Gold Catalysts: Aerobic and Anaerobic Hydroxymatairesinol Selective Dehydrogenation*, J. Mol. Catal. 2012 (*submitted*).

## List of Other Publications Related to the Topic

---

1. **O. A. Simakova**, M. Lopez, E. V. Murzina, I. Prosvirin, A. V. Simakov, D. Yu. Murzin. *Structure sensitivity of the lignan hydroxymatairesinol aerobic oxidation over Au/Al<sub>2</sub>O<sub>3</sub> catalysts*, in preparation.
2. **O. A. Simakova**, E. V. Murzina, J. Wärnå, D. Yu. Murzin. *Biomass derived lignan oxidation over gold catalysts: the reaction kinetics*, in preparation.
3. B. T. Kusema, B. C. Campo, **O. A. Simakova**, A.-R. Leino, K. Kordás, P. Mäki-Arvela, T. Salmi, D. Yu. Murzin. *Selective oxidation of D-galactose over gold catalysts*, ChemCatChem, 2011, 3, 1789-1798.
4. D. Yu. Murzin, **O. A. Simakova**, I. L. Simakova, V. N. Parmon. *Thermodynamic analysis of the cluster size evolution in catalyst preparation by deposition–precipitation*, React. Kinet. Mech. Cat., 2011, 104, 259–266.
5. I. L. Simakova, Yu. S. Solkina, B. L. Moroz, **O. A. Simakova**, S. I. Reshetnikov, I. P. Prosvirin, V. I. Bukhtiyarov, V. N. Parmon, D. Yu. Murzin. *Selective vapour-phase  $\alpha$ -pinene isomerization to camphene over gold-on-alumina catalyst*. Appl. Catal. A, 2010, 385 (1-2), 136-143.
6. K. Arve, J. Adam, **O. Simakova**, L. Čapek, K. Eränen, D. Yu. Murzin. *Selective catalytic reduction of NO<sub>x</sub> over nano-sized gold catalyst supported on alumina and titania and over bimetallic gold-silver catalyst supported on alumina*. Top. Catal. 2009, 52, 1762-1765.
7. **O. A. Simakova**, E. V. Murzina, J. Wärnå, D. Yu. Murzin. *Biomass derived lignan oxidation over gold catalysts*. //243rd American Chemical Society national meeting, San Diego, March 25-29, 2012, CATL 127.
8. **O. A. Simakova**, E. V. Murzina, P. Mäki-Arvela, S. M. Willför, D. Yu. Murzin. *Catalytic transformation of biomass derived lignan hydroxymatairesinol over gold catalysts*. //Russian national congress on catalysis, Moscow, October 3-7, 2011, OP-S-I-5.
9. **O. A. Simakova**, E. V. Murzina, K. Kordás, S. M. Willför, D. Yu. Murzin. *Synthesis of an active component in cosmetic, pharmaceutical and textile industry by selective oxidation of a biomass derived lignan over gold catalysts*. //International conference “5th IDECAT/ERIC J-CAT Conference on Catalysis”, Bertinoro (Bologna), September 22-25, 2011, SO31.
10. **O. A. Simakova**, E. V. Murzina, S. Davis, S. M. Willför, R. J. Davis R. J., D. Yu. Murzin. *Biomass processing over gold catalysts via selective oxidation of hydroxymatairesinol (HMR) and 5-hydroxymethylfurfural (HMF)*. //International conference “Renewable Wood and Plant Resources: Chemistry, Technology, Pharmacology, Medicine”, St. Petersburg, June 21-24, 2011.

11. **O. A. Simakova**, Yu. S. Solkina, P. Mäki-Arvela, I. L. Simakova. *Kinetic study of the catalytic transformation of biomass components over gold catalysts*. //XIX international conference on chemical reactors, September 5-9, 2010, Vienna, Austria, p. 559-560, PP-III-65.
12. **Simakova O.A.**, B. Kusema, B. Campo, P. Mäki-Arvela, A.-R. Leino, K. Kordás, D. Yu. Murzin. *Gold catalysts in the selective arabinose oxidation: size effect*. //International conference “Catalysis for renewable sources: fuel, energy, chemicals”, St. Petersburg, Tsars Village, Russia, June 28 - July 2, 2010, OP-2-9, p. 51.
13. **O. A. Simakova**, P. Mäki-Arvela, K. Kordás, D. Yu. Murzin. *Linoleic Acid isomerization over gold catalysts*. OP // The 5th International conference on gold science, technology and its applications, Heidelberg, Germany, July 26-29, 2009.

## Contents

---

<b>Preface .....</b>	<b>i</b>
<b>Abstract .....</b>	<b>iii</b>
<b>Referat .....</b>	<b>iv</b>
<b>Реферат .....</b>	<b>v</b>
<b>List of Publications.....</b>	<b>vi</b>
<b>List of Other Publications Related to the Topic.....</b>	<b>vii</b>
<b>Contents.....</b>	<b>ix</b>
<b>1. Introduction .....</b>	<b>1</b>
1.1. Biomass valorization .....	1
1.1.1. Polysaccharides-derived compounds .....	2
1.1.2. Extractives and their Derivatives .....	4
1.2. Catalysis by gold .....	6
1.3. Aim and scope of the research .....	8
<b>2. Experimental.....</b>	<b>9</b>
2.1. Materials.....	9
2.1.1. Substrates .....	9
2.1.2. Catalysts .....	9
2.2. Catalysts characterization techniques .....	10
2.2.1. Nitrogen adsorption.....	10
2.2.2. Fourier transmission infrared spectroscopy .....	11
2.2.3. Temperature-programmed desorption of carbon dioxide .....	11
2.2.4. Transmission electron microscopy .....	11
2.2.5. X-ray diffraction .....	11
2.2.6. Inductively coupled plasma optical emission spectroscopy and atomic emission spectroscopy .....	12
2.2.7. X-ray photoelectron spectroscopy .....	12
2.2.8. UV-vis spectroscopy .....	12
2.2.9. Temperature-programmed oxidation .....	12
2.2.10. Thermogravimetric analysis with differential scanning calorimetry	13
2.3. Reactor systems.....	13

2.3.1. Three-phase reactors .....	13
2.3.1.1. Linoleic acid isomerization.....	13
2.3.1.2. Selective oxidation of L-arabinose .....	13
2.3.1.3. Selective oxidation of hydroxymatairesinol .....	14
2.3.2. Two-phase reactors .....	14
2.4. Product analysis.....	15
2.4.1. Fatty acids .....	15
2.4.2. Monosaccharides and low-molecular weight compounds .....	15
2.4.3. Lignans .....	15
2.4.4. Products of ethanol selective oxidation .....	16
<b>3. Results and Discussion .....</b>	<b>17</b>
3.1. Characterization of catalysts .....	17
3.1.1. Support textural properties and Au particle size.....	17
3.1.2. Acidity and basicity of the support .....	21
3.1.3. Electronic state of gold species .....	23
3.2. Isomerization of linoleic acid [III] .....	24
3.3. Selective oxidation reactions.....	25
3.3.1. Gas-phase selective oxidation of ethanol [IV-VI] .....	25
3.3.2. Structure sensitivity of L-arabinose selective oxidation [VII] .....	27
3.3.3. Liquid-phase oxidation of the lignan hydroxymatairesinol [VIII-XI] .....	29
3.3.3.1. Effect of the solvent and the reaction atmosphere.....	29
3.3.3.2. Effect of the catalyst support and active phase.....	31
3.3.3.3. Catalyst deactivation and regeneration .....	34
3.3.3.4. Reaction kinetics .....	35
3.3.3.5. Structure sensitivity .....	38
3.3.3.6. Reaction mechanism .....	40
<b>4. Conclusions .....</b>	<b>44</b>
<b>Notations.....</b>	<b>45</b>
<b>References .....</b>	<b>46</b>
<b>Original Publications.....</b>	<b>51</b>

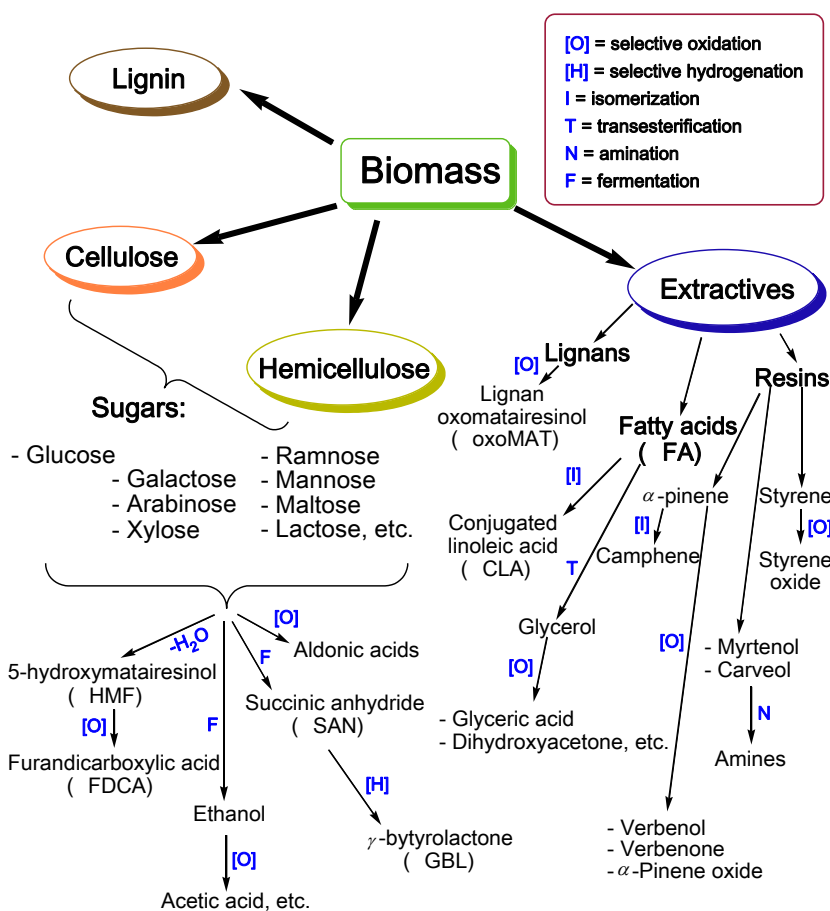
# 1. Introduction

---

## 1.1. Biomass valorization

Biomass is a rich renewable feedstock for fine chemicals, polymers, and a variety of commodities replacing petroleum-derived chemicals. It was stated a decade ago, that the use of biorenewable feedstock will provide the sustainable development of the chemical industry [1-3]. The main components of wood biomass are cellulose (40-50 %), lignin (16-33 %), hemicelluloses (15-30 %), and extractives (1-10 %) [4]. Lignin and cellulose transformation has been studied extensively, while less attention has been paid to hemicelluloses and extractives, which are important feedstocks for commodities and fine chemicals. The essential part of renewables is produced from factory waste. An example of this is pulp and paper production, which is one of the most important sectors of the forest-based industry. Initially, wood chips undergo a selection procedure to separate them from knots and bark, which are undesirable for paper and board production. These parts of trees, normally considered as waste, contain extractives valuable for chemical synthesis, the main components being resin acids, terpenes, sterols, phenolic substances (particularly lignans), sugars, etc. The conversion of biomass into diverse valuable chemicals is the key concept of a biorefinery.

Catalytic conversion of biomass which reduces the use of toxic chemicals is one of the important approaches to improve the profitability of biorefineries. Various opportunities to transform biomass were reviewed some years ago [4-8]. The routes of catalytic transformations include chemical reactions, such as selective oxidation, hydrogenation and isomerization, which can be performed using gold catalysts. Scheme 1 shows the explored opportunities to apply gold catalysts in biomass-derived chemicals valorization. Utilization of gold catalysts for biomass conversion is a promising direction, since value-added chemicals can be produced in many reactions, for which gold has demonstrated an outstanding activity and selectivity.



**Scheme 1.** Routes of biomass-derived compounds transformation over gold catalysts.

### 1.1.1. Polysaccharides-derived compounds

Cellulose and hemicelluloses represent the largest part of wood biomass (55-80%) [4]. These polysaccharides consist of sugar units, linked to each other by glycosidic bonds. Cellulose is a linear polysaccharide consisting of linked D-glucose units, while hemicelluloses are heteropolysaccharides consist of a large number of different sugar units, pentoses and hexoses (Figure 1). Monomeric sugar units obtained by hydrolysis of cellulose and hemicelluloses and their derivatives can be catalytically transformed into a wide spectrum of value-added chemicals.



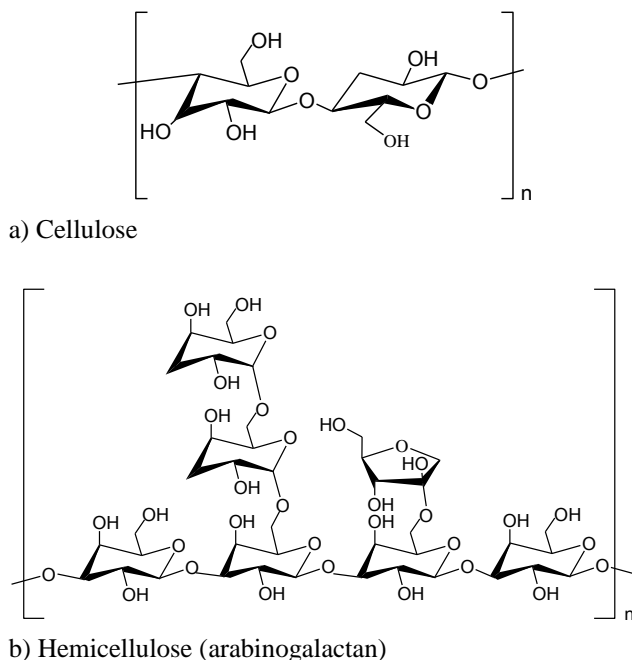


**Figure 1.** Structure of polysaccharides.

L-Arabinose and D-galactose obtained by hemicelluloses (i.e. arabinogalactans) hydrolysis, which appear in large amounts in larch species [9], can be selectively oxidized to arabinonic and galactonic acids, respectively. These aldonic acids are valuable in different industrial applications, such as, the food industry, cosmetics and medicine [10].

Biomass-derived sugars and their derivatives are important organic platform molecules. Agricultural waste is an attractive feedstock for bioethanol production, since lignocellulosic substances are renewable and abundant. Efficient pretreatment before total delignification of lignocellulosics increases the concentration of fermentable sugars. Another way to make process cost-effective is the development of novel fermentation technologies [11]. Selective oxidation of bioethanol results in the formation of various valuable products, such as acetaldehyde, 1,1-diethoxyethane, acetic acid and ethyl acetate. Acetic acid is a commodity in chemical syntheses, including vinyl acetate production for further manufacturing of polyvinyl acetate.

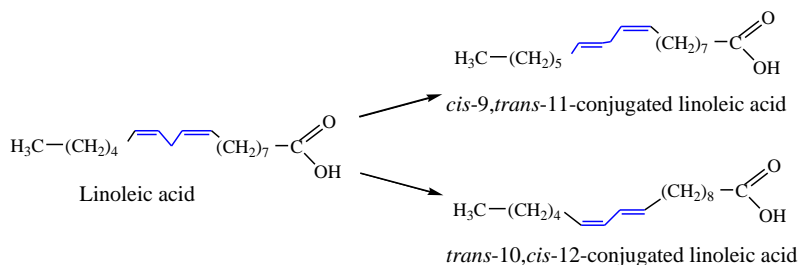
Currently acetic acid is produced via methanol carbonylation utilizing fossil resources exclusively [12]. Ethyl acetate has a wide range of applications in different areas, including the paint and food industries [13]. Gold catalysts have been found to be active and selective in the synthesis of both, acetic acid and ethyl ester, in the presence of oxygen [14, 15]. Moreover, application of gold catalysts has allowed the use of less drastic conditions than in the case of other catalysts active in these reactions, such as supported Pt, Pd, Ru, or  $V_2O_5$ , Nb-Mo-V-Ox, etc. [16-18].

### 1.1.2. Extractives and their Derivatives

#### Fatty acids

Tall oil is the by-product from the Kraft pulping process. Crude tall oil (CTO) contains mainly fatty acids and resin acids, as well as sterols, etc. Vacuum distillation of CTO gives the following products: tall oil fatty acids (TOFA) (16-30%), tall oil resin (TOR) (25-35%), distilled tall oil (DTO) (6-10%), light oil (10-12%), and pitch (20-30%) [19]. The product mixture obtained from CTO fraction of TOFA consists of fatty acids ( $C_6$ - $C_{20}$ ), where the main one is linoleic acid.

Linoleic acid, an unsaturated fatty acid, is abundant in vegetable oils comprising safflower, grape seed, poppyseed, and sunflower oil. Linoleic acid ( $C_{18}:2$ ) has two double bonds located on carbon atoms 9 and 12, both in *cis* configuration, and they can be isomerized through double bond migration to conjugated linoleic acids (CLA) (see Scheme 2).



**Scheme 2.** Isomerization of linoleic acid to biologically active conjugated linoleic acid isomers (CLA).

These isomers are well known for their strong anticarcinogenic effect discovered in 1987 by Pariza and co-workers [20], as well as reducing body fat activity [21]. Health benefits are attributed to the presence of *cis*-9,*trans*-11 and the *trans*-10,*cis*-12 isomers [22-24]. The industrially attractive source for CLA production is poppy (77%), safflower (75%), cucumber (72%), grapeseed (70%), linola flaxseed (72%) and others [25].

Synthesis of CLA was performed under alkaline conditions [26], where 90% of the product was mixture of *cis*-9,*trans*-11, *trans*-10,*cis*-12, *trans*-9,*trans*-11, *trans*-10,*trans*-12 isomers, and 10% of *cis*-9,*cis*-11, *trans*-9,*cis*-11, *cis*-10,*cis*-12, *cis*-10,*trans*-12, *cis*-11,*cis*-13 isomers. Homogeneously catalyzed linoleic acid isomerization utilizing tris(triphenylphosphine)chlororhodium [27] and arene chromiumcarbonyl complexes [28] enable reactor temperatures lower than 180-200°C.

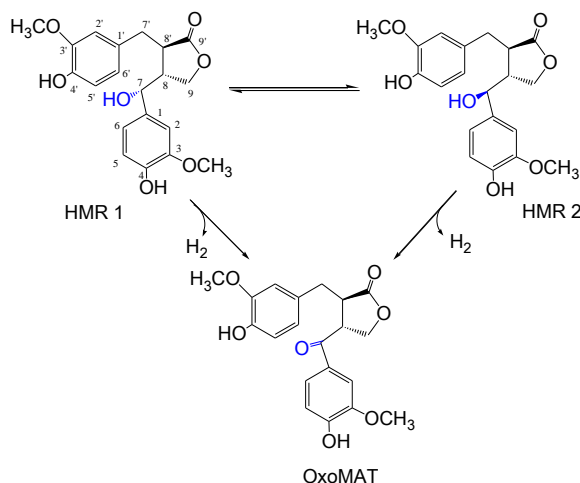
Homogeneously catalyzed synthesis of conjugated linoleic acid isomers (CLA) synthesis comprises the utilization of alkali and an organic solvent, which has drawbacks from both an ecological and economic point of view. Moreover, separation of the catalyst is challenging. These difficulties can be solved by heterogeneous catalysis. However, for the successful reaction performance preadsorbed hydrogen is needed on the catalyst surface. Thus, the application of traditional catalysts (e.g. ruthenium) is difficult due to the hydrogenation products formation (oleic and stearic acids) [29]. However, a high activity and selectivity of

ruthenium catalysts has been later reported in [30]. Since gold catalysts are less active in the hydrogenation compared to Ru based catalysts, a higher selectivity of these catalysts could be anticipated.

### Lignans

Lignans are a group of natural phenolic compounds found in different parts of plants, such as wooden parts, roots, leaves, stem, seeds, flowers and fruits. Coniferous trees contain a large number of different lignans in an unconjugated form, with the kind and amount of lignans depending on the species and part of the tree. For example, Norway spruce (*Picea abies*) knots contain large quantities of lignans, among which hydroxymatairesinol (HMR) [31-33] is the most abundant. The lignan HMR, constituting 65-85 wt. % of the total lignans, appears in unconjugated free form [34], simplifying the isolation process. Extracted from wood biomass, HMR is a mixture of two diastereomers, namely (7R,8R,8'R)-(-)-7-*allo*-hydroxymatairesinol (HMR 1 or RRR-HMR) and (7S,8R,8'R)-(-)-7-*allo*-hydroxymatairesinol (HMR 2 or SRR-HMR), the ratio of which depends on the feedstock, HMR 1 and HMR 2 can be isomerized into each other. The ratio between HMR 1 and HMR 2 depends on the feedstock.

Lignans have been shown to provide benefits for the human health, for example, a lignan-rich diet decreases the risk for various cancers and cardiovascular diseases [35]. In addition to anticarcinogenic effects, lignans are proven to have antioxidative effects [36-38]. Evaluation of the radical and superoxide scavenging activities of lignans have shown that lignan oxomatairesinol (oxoMAT) exhibits the highest superoxide scavenging activity. Therefore, lignan oxoMAT and its derivatives, due to their antioxidative activity [39] and UV-protection properties [40], can be applied for cosmetic and pharmaceutical uses (skin- and hair-care products), as well as color-keeping agents for the textile industry. However, oxoMAT cannot be extracted in considerable amounts from wood biomass, while it can be synthesized by selective dehydrogenation of HMR (Scheme 3).

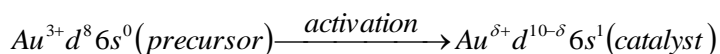


**Scheme 3.** Catalytic transformation of hydroxymatairesinol (HMR) to oxomatairesinol (oxoMAT).

The formation of oxoMAT by light-irradiation from HMR was reported in [41], while in [42] 2,3-dichloro-5,6-dicyano-1,4-benzoquinone (DDQ) was used as an oxidizing agent. As a first attempt to perform the reaction via heterogeneous catalysis, more attractive for industrial process, Pd/C catalysts have been studied for the synthesis of oxoMAT in anaerobic conditions and by using organic solvents. However, oxoMAT was not the only product in this reaction [43]. There is no additional information available about this synthesis being carried out over heterogeneous catalysts, despite an evident need for an industrially applicable catalytic method for the selective synthesis of this lignan.

## 1.2. Catalysis by gold

Gold was regarded as catalytically inert metal until the discovery of Haruta and co-workers, who were the first to demonstrate the catalytic activity of gold catalysts in low-temperature CO oxidation [44]. A remarkable activity of nanosized gold catalysts in oxygen-atom transfer reactions was further shown in numerous reactions of selective oxidation of a variety of organic molecules, such as alcohols and aldehydes [45, 46], alkanes [47], olefins [48, 49] and polyfunctional alcohols [50-52]. The main advantage of gold-based catalysts is environmentally-friendly manufacturing of organic chemicals employing molecular oxygen or air as oxidizing agents and relatively mild reaction conditions. Moreover, compared to typically applied platinum and palladium catalysts gold is more stable under an oxidative atmosphere. However, the mechanism of catalysis by gold and oxygen activation is still a matter of debate. In [53], a mechanism of gold activation was proposed, where the possible catalytic active sites are considered to be formed during the activation treatment, being partially oxidized gold ( $Au^{\delta+}$ ) with unoccupied outer d orbitals, similar to the electronic structure of Pt. Thus, the formation of active centers via activation treatment is the result of electronic structure changes:



It is generally accepted that the catalytic activity of gold catalysts is strongly dependent on the gold particle size [54]. In [55, 56], it was pointed out that the largest effect on the activity is attributed to the presence of low-coordinated gold atoms, which are abundant in the smallest gold nanoparticles. The most reactive atoms are located at the edges and corners of the particles. These Au atoms are suggested to be able to facilitate the adsorption of CO and dioxygen to perform the CO oxidation. The number of low-coordinated corner and edges sites is decreasing with an increasing Au particle size. Therefore, even when the particle size is slightly changing, the fraction of active sites decreases dramatically. In particular, the fraction of corners increases significantly, when the particle size is less than 4 nm and scales approximately  $d^{-3}$  as the diameter of the particle decreases [56]. The other effects, such as interactions with the support [57, 58], charge transfer [59], strain [60] may also contribute, but to a lesser extent.

Activation of molecular oxygen on gold particles is a crucial step in the oxidation reactions. Low-temperature activation of dioxygen in CO oxidation was studied in [61]. The results

suggested that dioxygen is adsorbed on gold clusters, forming a superoxide ( $\text{O}_2^-$ ), which is the activated form of oxygen. Moreover, it was also observed, that adsorbed oxygen enhances the adsorption of the substrate (CO) on the gold particles.

Gold catalysts have also been evaluated in other reactions [62]. Since gold is less active in hydrogenation than conventional catalysts as Pt, Pd, Ni, and a number of other metals, Au based catalysts were found to be more efficient in some reactions involving hydrogen, where the selectivity is an issue. For example, gold catalysts were shown to be active and selective in the hydrogenation of various molecules, such as olefins and dienes [63], the carbonyl group of  $\alpha$ - $\beta$ -unsaturated aldehydes [64, 65], nitro groups [65, 66]. The unique properties of nanosized gold to activate oxygen and facilitate weak bounding of hydrogen allow gold catalysts to be successfully employed in a number of fine chemicals synthesis reactions, such as partial oxidation and hydrogenation. Gold as a catalyst can be applied in similar transformations of biomass-derived compounds into value-added chemicals.

### **1.3. Aim and scope of the research**

The aim of the thesis was to investigate catalytic transformations of biomass-derived compounds into value-added chemicals over heterogeneous gold catalysts. Supported gold and gold-palladium catalysts were prepared and evaluated in several reactions, such as linoleic acid isomerization; selective oxidations of ethanol, L-arabinose, and the lignan hydroxymatairesinol. The research was focused on the development of catalytic biomass processing based on the understanding of the fundamental catalytic process and reaction kinetics. Preparation of Au/C catalysts methods and their applications are described in review [I]. Biomass transformations over gold catalysts are reviewed in [II]. Other publications address the studied reactions in more detail. Linoleic acid isomerization over gold catalysts was studied in article [III], while the results on selective oxidation of ethanol were summarized in articles [IV-VI]. Among many issues associated with oxidation of sugars the specific interest was on the structure sensitivity in L-arabinose oxidation [VII]. Selective oxidation of the lignan hydroxymatairesinol (HMR) over gold catalysts was extensively investigated in articles [VIII-XI]. The reaction kinetics and the structure sensitivity of the selective oxidation of HMR were also studied, covering such aspects as the catalyst selection, reaction kinetics, structure sensitivity, application of bimetallic catalysts, catalyst deactivation and the reaction mechanism.

Information acquired from this investigation was used for the interpretation of the reaction mechanism and catalytic effects. The data can be subsequently applied in the catalyst design, process design and optimization. The experiments for gas-phase ethanol oxidation were carried out in a continuous mode at Boreskov Institute of Catalysis. The selective oxidation of L-arabinose was conducted in a tailor-made shaker reactor, while the isomerization of linoleic acid and the selective oxidation of HMR were performed in a glass reactor equipped with an impeller.

## 2. Experimental

### 2.1. Materials

#### 2.1.1. Substrates

Most of the efforts were put on investigation of biomass, such as L-arabinose and the lignans. However, compounds derived directly from model substrates were also examined. Linoleic acid ( $C_{18}H_{32}O_2$ ) of 99 % purity was supplied by Sigma-Aldrich (Germany). The isolated *trans*-10,*cis*-12, *cis*-9,*trans*-11, *cis*-9,*cis*-11, and *trans*-9,*trans*-11 isomers of CLA ( $C_{18}H_{32}O_2$ ) of 99 % purity were supplied by Matreya Inc. (USA). L-Arabinose (99.9 %) was supplied by Danisco. Lignan hydroxymatairesinol (HMR) was prepared at the Laboratory of Wood and Paper Chemistry at Åbo Akademi University. HMR was isolated from Norway spruce (*Picea abies*) knots as described in [67]. Lignans were extracted from ground knots by an acetone-water mixture. The extract was concentrated in a rotary evaporator and then purified by flash chromatography. Two diastereomers of HMR, (7R,8R,8'R)-(-)-7-*allo*-hydroxymatairesinol (HMR 1 or RRR-HMR) and (7S,8R,8'R)-(-)-7-*allo*-hydroxymatairesinol (HMR 2 or SRR-HMR), were obtained as a mixture with the ratio between them HMR 2:HMR 1 = 2:1 mol/mol. The purity of HMR was determined by GC to be 95 %. The major contaminants were the lignans  $\alpha$ -conidendrin and  $\alpha$ -conidendric acid.

The solvent applied in linoleic acid isomerization was *n*-decane of 95.5 % purity (Fluka, Switzerland). The lignan HMR oxidation was studied utilizing as solvents 2-propanol (Sigma-Aldrich, 99.8 %), ethanol (Altia Corporation, 99.5 %), 1-butanol (Acros, 99 %), and 2-pentanol (The British Drug Houses Ltd., 95 %), cyclohexanol (J. T. Baker, 99 %), 1,4 – dioxane (Labscan, 99.8 %), tetrahydrofuran (THF) (Labscan, 99.8 %), and their mixtures with de-ionized water.

#### 2.1.2. Catalysts

Several methods of gold catalysts preparation were applied: direct ion exchange (DIE) of the gold species with the hydroxyl groups of the support surface followed by washing with an aqueous ammonia solution as described in [68], and deposition-precipitation with urea (DPU) [69]. To prepare carbon-supported gold catalysts, the immobilization of PVA stabilized gold sols by a carbon support (Sibunit) was applied [70]. Mesoporous carbonaceous material Sibunit was applied as a support. The following metal oxide supports were purchased:  $Al_2O_3$  (UOP, A-201),  $TiO_2$  (Degussa AG, Aerolyst 7708, anatase > 70 %),  $SiO_2$  (Merck), and MgO (Sigma-Aldrich, 99 %). Aqueous solutions of  $HAuCl_4$  (99.9 % ABCR, Darmstadt) were utilized as a metal precursor. Urea (99.5 % purity) was supplied by Sigma-Aldrich. The detailed synthesis procedures for gold supported on C,  $Al_2O_3$ ,  $SiO_2$ ,  $TiO_2$ , MgO can be found in the publications [III-VIII]. 2 wt. % Au/ $Al_2O_3$  was prepared by DPU and DIE methods, changing several catalyst preparation parameters, such as the washing agent (ammonia or water), the concentration of the precursor solution, and the calcination temperature (300-600°C), which gave a possibility to vary the gold particle size [VII].

Gold and gold-palladium catalysts supported on different metal oxides described below were prepared in collaboration with Centro de Nanociencias y Nanotecnologia, Universidad

Nacional Autónoma de México (CNyN-UNAM). Commercial  $\text{CeO}_2$ ,  $\text{Al}_2\text{O}_3$ ,  $\text{ZrO}_2$ ,  $\text{La}_2\text{O}_3$  (Alfa-Aesar),  $\text{MgO}$  (Mallinckrodt Baker, Inc.) oxides were used as supports. The alumina support applied in this set of catalysts was further noted as  $\text{Al}_2\text{O}_3$ -I. Gold (3 wt. %) was first deposited on the supports by the DPU technique using  $\text{HAuCl}_4$  (Alfa-Aesar) as a gold precursor and urea as a precipitation agent according to [71]. Bimetallic Au-Pd catalysts were prepared as described in article [IX] using  $\text{PdCl}_2$  (Alfa-Aesar). Before catalytic tests, the samples were reduced at  $350^\circ\text{C}$  under hydrogen flow with a ramp rate of  $20^\circ\text{C}/\text{min}$ .

Nanostructured alumina named hereafter as  $\text{Al}_2\text{O}_3$ -II, mixed Ce-Al-O oxides with the ceria contents of 10 and 30 wt.% and Ce-Zr-Al-O with the content of ceria-to-zirconia ratio of 5:5 and 15:15 wt. % were prepared by the sol-gel method from organo-metallic precursors following a procedure reported previously [72]. Gold (3 wt. %) was supported on the nanostructured  $\text{Al}_2\text{O}_3$ , Ce-Al-O and Ce-Zr-Al-O oxides by the DPU method. The supports in this serie will be further named according to the metal element in the metal oxide composition, as Al, Ce, Zr. The mixed support and catalyst samples are coded as Ce(N)-Al, Ce(N)Zr(N)-Al and Au/Ce(N)-Al, Au/Ce(N)Zr(N)-Al where N manifests the ceria or zirconia content (5, 10, 15 or 30 wt. %), respectively. Before catalytic tests, the samples were reduced at  $350^\circ\text{C}$  under hydrogen flow with a ramp rate  $20^\circ\text{C}/\text{min}$ . The details of catalysts preparation procedures are given in article [IX].

## **2.2. Catalysts characterization techniques**

Catalysts characterization was performed in order to understand the influence of the physical and chemical properties of the catalysts on the catalytic behavior. The catalysts were characterized by nitrogen adsorption, Fourier transmission infrared spectroscopy (FTIR) using pyridine as a probe molecule, temperature-programmed desorption of  $\text{CO}_2$  ( $\text{CO}_2$ -TPD), transmission electron microscopy (TEM), X-ray diffraction (XRD), inductively coupled plasma optical emission spectroscopy (ICP-OES) and atomic emission spectroscopy (ICP-AES), X-ray photoelectron spectroscopy (XPS), UV-vis spectroscopy, temperature-programmed oxidation (TPO), and thermogravimetric analysis with differential scanning calorimetry (DSC-TGA). Catalysts characterization was performed at Åbo Akademi University (nitrogen adsorption, XPS, FTIR,  $\text{CO}_2$ -TPD, ICP-OES, DSC-TGA) as well as in collaboration with University of Oulu (TEM, XRD), University of Limerick (XPS) and CNyN-UNAM (nitrogen adsorption, TEM, ICP-AES, UV-vis spectroscopy). Although some measurements were performed using different equipment, the same analytical procedures were kept.

### **2.2.1. Nitrogen adsorption**

A Carlo Erba sorptometer 1900, Gemini 2600 Micromeritics and TriStar II Micromeritics unit device were utilized in the measurements of the surface area and the micropore volume by nitrogen physisorption. The specific surface area of the samples was determined using the BET equation. Before analysis, the samples were either evacuated at  $400^\circ\text{C}$  for 4 h prior to analysis, or heated at  $300^\circ\text{C}$  in argon flow for 1 h.



### 2.2.2. Fourier transmission infrared spectroscopy

The acidities of the supports were determined by Fourier transformed infrared spectroscopy (FTIR) using pyridine as a probe molecule. Thin self-supporting wafers of the adsorbents were prepared by pressing and they were placed in the cell. The cell was evacuated to  $\sim 10^{-6}$  Torr at 450°C for 1 h. Thereafter, the cell was cooled to 100°C and the background (Bkg) spectra were taken as an average of accumulated 100 scans over the frequency range of 4000–400  $\text{cm}^{-1}$ . Pyridine was then adsorbed onto the sample at 100°C for 30 min. The subsequent desorption was performed at 250°C, 350°C, and 450°C. The spectra were recorded between each temperature ramp at 100°C. The adsorption bands around 1610 and 1450  $\text{cm}^{-1}$  characterize Lewis acid sites, while the adsorption signals at 1545 and 1630  $\text{cm}^{-1}$  correspond to the Brønsted acidity of the adsorbent [73].

### 2.2.3. Temperature-programmed desorption of carbon dioxide

The basicities of magnesia, titania and alumina were measured by temperature-programmed desorption of  $\text{CO}_2$  ( $\text{CO}_2$ -TPD) using Micromeritics AutoChem 290. The measurements were performed in a conventional flow-through reactor with  $\text{CO}_2$  as the probe molecule. 250 mg of the metal oxide was flushed with a stream of helium (100 ml/min) to clean the sample at 550°C for 30 min before cooling to 50°C. A stream of  $\text{CO}_2$  was allowed to saturate the solid particles for 30 min, thereafter the weakly bound  $\text{CO}_2$  and other physisorbed molecules were removed by a stream of pure He for 1 h. Chemisorbed  $\text{CO}_2$  was desorbed by heating to 900°C (ramp of 10 C/min), while He was used as a carrier gas. The effluent from the reactor was analyzed by a TC detector.  $\text{CO}_2$  calibration was performed by a pulse injection of 1 ml  $\text{CO}_2$  to determine the actual amount of  $\text{CO}_2$  desorbed from magnesia.

### 2.2.4. Transmission electron microscopy

Electron microphotographs of the samples were taken with a LEO 912 OMEGA energy-filtered transmission electron microscope by using 120 kV acceleration voltage and JEOL 2010 microscope. Histograms of the particle size distribution were obtained by counting more than 200 particles on the micrographs for each sample. The mean diameter ( $d_m$ ) of the particles was calculated using the well-known procedure of particle size distribution histograms with the following equation:

$$d_m = \frac{\sum_i (x_i d_i)}{\sum_i x_i},$$

where  $x_i$  is the number of particles with diameter  $d_i$ .

### 2.2.5. X-ray diffraction

X-Ray diffraction was performed by using  $\text{CuK}\alpha$  radiation (Siemens D5000 diffractometer equipped with a graphite monochromator to suppress fluorescent and  $\text{Cu-K}\beta$  radiation). The average crystallite size of the gold catalyst particles was estimated using the Scherrer's equation from the peak half-widths of the Au(111) reflection measured at  $2\Theta \sim 38.3^\circ$ .

Instrumental broadening and unresolved  $\text{CuK}\alpha 1$  and  $\alpha 2$  radiation were neglected (the error was less than 2 %).

### **2.2.6. Inductively coupled plasma optical emission spectroscopy and atomic emission spectroscopy**

The metal loading was determined by inductively coupled plasma-optical emission spectroscopy (ICP-OES) with a PerkinElmer, Optima 5300 DV spectrometer. For this purpose, 60 mg of the sample were treated with 5 ml of *aqua regia*, digested in a microwave oven, diluted to 100 ml and analyzed by the spectrometer.

The obtained gold catalyst samples were chemically analyzed with an inductively coupled plasma atomic emission spectroscopy (ICP-AES) using a Varian Liberty 110 ICP Emission Spectrometer. Typically, 30 mg of the catalyst was dissolved in 20 ml of ( $\text{H}_2\text{SO}_4\text{:HCl:HNO}_3 = 6\text{:}6\text{:}3$ ) acids and the sample was heated to 150°C.

### **2.2.7. X-ray photoelectron spectroscopy**

The XPS measurements were carried out with a PHI Quantum 2000 Scanning ESCA Microprobe spectrometer equipped with an Al anode. Gold supported on  $\text{TiO}_2$ ,  $\text{Al}_2\text{O}_3$  and  $\text{SiO}_2$  was analyzed as a powder mounted in a double-sided adhesive tape. The survey and multi spectra were collected at 187.75 eV and 11.75 eV pass energy, respectively. During the analysis, electron and ion beams were applied over the catalyst to compensate the charge effect. Spectra deconvolution was performed with the free software XPS Peak 4.1. A combination of 30% Lorentzian and 70% Gaussian curves was fitted after subtraction of the Shirley background. For quantitative analysis, the peaks areas were corrected for the corresponding sensitivity factors.

XPS data were also obtained with a Kratos AXIS 165 spectrometer using the monochromatic  $\text{AlK}\alpha$  radiation ( $h\nu=1486.58$  eV) and a fixed analyzer pass energy of 20 eV. All measured binding energies (BE) were referred to the C1s line of adventitious carbon at 284.8 eV. The spectrum deconvolution was done with a background estimation using Shirley software.

### **2.2.8. UV-vis spectroscopy**

UV-Visible diffuse reflectance spectra (UV-Vis DRS) were recorded at the room temperature for gold samples treated in  $\text{H}_2$  at 350°C using a Varian Cary 300 scan spectrophotometer equipped with a standard diffuse reflectance unit. Teflon PTF Halon (Varian) was used as a reference. Each UV-Visible DR spectrum was obtained by subtraction of the fresh sample spectrum from the spectrum for the sample after treatment.

### **2.2.9. Temperature-programmed oxidation**

Spent catalysts were also analyzed by the TPO method. For this purpose, 200 mg of the sample were placed in a quartz tube reactor and heated in an oxidizing atmosphere (2.5 %  $\text{O}_2$  in He gas mixture, supplied by AGA) in the temperature range of 30-650°C. The organic compounds from the outlet were analyzed by mass-spectrometry (Quadrupole mass spectrometer QMS 200). Predominantly,  $\text{CO}_2$  and CO were analyzed to perform the gas calibration.

### 2.2.10. Thermogravimetric analysis with differential scanning calorimetry

Thermogravimetric analysis was performed with DSC-TGA (Q Series instrument) by subjecting ca. 9 mg of the spent catalyst to 400°C and 500°C at 2°C min<sup>-1</sup> under a steady stream of 20 % oxygen in a nitrogen gas mixture at 100 ml/min.

## 2.3. Reactor systems

Experiments were carried out in different laboratory-scale reactor set-ups. Utilized reactors are suitable to provide data for studying the mechanism and kinetics of the reactions, which is important for process simulation and catalyst design. The employed reactor systems facilitate the evaluation of the catalytic activity, in the absence of heat and mass transfer limitations.

### 2.3.1. Three-phase reactors

Linoleic acid isomerization and selective oxidation of HMR were carried out in a semi-batch glass reactor. The experiments were performed in the kinetic regime. The catalyst grain size was 45–63 µm to suppress the internal mass transfer limitations. Furthermore, the reaction mixture was stirred at 1000 rpm to suppress external mass transfer limitations, L-arabinose oxidation was conducted in a semi-batch mode tailor-made shaker reactor equipped with in-situ catalyst potential measurement and a pH controller.

#### 2.3.1.1. Linoleic acid isomerization

The isomerization experiments were carried out in a 200 ml stirred glass reactor, which was equipped with a reflux condenser and a heating jacket [III]. The catalyst (fractions of catalysts below 70 µm and 40–63 µm, respectively, to suppress the internal diffusion) was introduced into the reactor, preactivated under hydrogen flow (100 ml/min) at 150°C for 1 h. An amount of 200 mg of linoleic acid was mixed with 70 ml of the solvent in a glass drip funnel. The amounts of the catalyst and the substrate were chosen following the previous work which reported the best results for the linoleic acid isomerization performance over Ru/C catalysts [74]. Such conditions correspond to the substrate-to-metal molar ratio equal to 14 mol/mol. The air above the reaction mixture and dissolved in the liquid phase was purged out by a nitrogen flow of 100 ml/min. The isomerization reaction was conducted at 150°C under a stirring speed of 1000 rpm to eliminate the external mass transfer resistance. Samples were withdrawn from the reactor at certain intervals through a sampling valve.

#### 2.3.1.2. Selective oxidation of L-arabinose

The catalyst evaluation was carried out in a semi-batch reactor [VII]. The catalysts were sieved to particle sizes of 45–63 µm to facilitate the absence of internal mass transfer limitations. The catalyst suspended in de-ionized water, was pre-reduced in situ by hydrogen (AGA, 99.999%) at 60°C during 10 min. An aqueous solution of L-arabinose was introduced into the reactor; and 100 ml 0.1 M solution of arabinose. The oxygen flow rate through the reactor was 2.5 ml/min diluted in 17.5 ml/min of nitrogen. The pH was kept at 8, by the addition of a 2.5 M NaOH solution using an automatic titration device (Metrohm Titrino 751).

The stainless steel reactor walls were utilized as an electrode collector for the measurements of the catalyst potential. Application of catalyst potential measurements is in particular advantageous in the oxidation reactions over metals as discussed by Mallat and Baiker [75]. The potential measurements were performed by means of an Ag/AgCl/3M KCl electrode. More details on the reaction performance and reaction set up can be found in ref. [76].

#### **2.3.1.3. Selective oxidation of hydroxymatairesinol**

The reaction was performed under atmospheric pressure in a stirred 200 ml glass reactor, equipped with a heating jacket (using silicon oil as the heat transfer medium), a re-flux condenser (cooling medium set -20°C), an oil lock, a pitched-blade turbine and stirring baffles. In a typical experiment, 250 mg of catalyst were put into the reactor in case of gold catalysts and 100 mg in case of palladium. To study the support activity, the corresponding amount of the support was charged into the reactor. The catalysts were pre-activated *in-situ* by heating under hydrogen (AGA, 99.999%) flow (100 ml/min) until 120°C, thereafter the reactor was cooled down to the reaction temperature 70°C under nitrogen (AGA, 99.999 %) flow (100 ml/min). To perform the reaction over palladium catalysts, 2-propanol was applied as a solvent. Gold catalysts were studied in different alcohols, mixtures of which (ethanol, 2-propanol, 1-butanol, and 2-pentanol, cyclohexanol) with de-ionised water were used as solvents. 1,4-Dioxane and tetrahydrofuran (THF), mixed with water were applied as solvents as well. The reactant solution (100 ml) with an HMR concentration of 1 mg/ml was poured into the reactor. The gas flow was changed to synthetic air, except for the case of dehydrogenation *per se* over palladium and gold catalysts, where the reaction was performed under a nitrogen flow. The stirring was started at the reaction time set to zero and the first sample was withdrawn. The reaction performance is described in detail in articles [VIII-X].

#### **2.3.2. Two-phase reactors**

Gas-phase ethanol oxidation was performed in collaboration with the Laboratory of Selective Heterogeneous Oxidation at Boreskov Institute of Catalysis. The temperature programmed gas-phase oxidation was performed in a quartz tube flow reactor with an internal diameter of 6 mm using shaped catalyst granules ( $d = 0.25\text{--}0.5$  mm; 500 mg). The gas mixture (EtOH/O<sub>2</sub>/He = 1/9/40; GHSV = 3600 h<sup>-1</sup>) was fed into the reactor filled with the catalyst; the reactor was operated under atmospheric pressure. The reaction temperature was measured inside the reactor ( $\pm 1^\circ\text{C}$ ), using a thermocouple inserted into the catalyst bed. The heating rate was 2°C/min. Prior to the kinetic measurements, the catalysts were activated in the reactor at 300°C in a flow of O<sub>2</sub>/He (1:3) for 1 h. The reactor was then cooled to 80°C and the feed was switched at this temperature to the reactant gas mixture for 20–30 min in order to reach well-defined steady state initial conditions [IV-VI].

## 2.4. Product analysis

### 2.4.1. Fatty acids

The samples from the semi-batch reactor were analyzed by temperature-programmed gas chromatography (GC, Hewlett Packard 6890 Series) using 50 m HP-5 column (inner diameter: 0.20 mm, film layer: 0.11  $\mu\text{m}$ ) and a flame ionization detector (FID) operating at 300°C. Prior to the GC analysis, the samples were silylated using N,O-bis(trimethylsilyl)trifluoroacetamide (BSTFA) and trimethylchlorosilane (TMCS) at 60°C, both supplied by Fluka (Switzerland). Details on the samples analysis can be found in article [III]. The retention times of the main components were following: linoleic acid - 11.95 min, stearic acid - 12.34 min, *cis*-9, *trans*-11 linoleic acid isomer-12.53 min, *cis*-11, *trans*-13 linoleic acid isomer - 12.65 min, *cis*-9, *cis*-11 linoleic acid isomer - 12.87 min, *trans*-9, *trans*-11 linoleic acid isomer - 13.05 min.

### 2.4.2. Monosaccharides and low-molecular weight compounds

To monitor the L-arabinose oxidation reaction, aliquots of the reaction mixture were taken at determined time intervals and analyzed by high precision liquid chromatography (HPLC), equipped with a Bio-Rad Aminex HPX-87C carbohydrate column. The Bio-Rad Aminex HPX-87°C column was connected to a refractive index (RI) detector and the column temperature of 80°C and 1.2 mM  $\text{CaSO}_4$  eluent flow rate of 0.4 ml/min were applied. For the Aminex cation H<sup>+</sup> column, HPX-97H, the mobile phase 5.0 mM  $\text{H}_2\text{SO}_4$  with a flow rate of 0.5 ml/min used and the column temperature was set at 65°C. The filtered samples were injected into the HPLC directly after the experiments without any pretreatment [VII].

### 2.4.3. Lignans

Samples were withdrawn from the reactor at different time intervals and analyzed by gas chromatography (GC) using an HP-1 column (length 25 m, inner diameter 0.20 mm, film thickness 0.11  $\mu\text{m}$ ) and a flame ionization detector (FID) operating at 300°C. For the analysis, 100  $\mu\text{l}$  (concentration of 1 mg/ml) of the sample was taken, and 2 ml of the internal standard for the GC containing betulinol (0.02 mg/ml) and C21:0 fatty acid (0.02 mg/ml) dissolved in methyl *tert*-butyl (MTBE,  $\text{C}_5\text{H}_{12}\text{O}$ ) was added. Samples were placed in a water bath at 40°C, where the MTBE and solvent were evaporated in a stream of nitrogen. Thereafter, the samples were dried in an oven at 40°C under vacuum for 20 min. The prepared samples were silylated prior to the analysis as follows: dried samples were dissolved in the silylation mixture of N,O-bis(trimethylsilyl)trifluoroacetamide (BSTFA), trimethylchlorosilane (TMCS) and pyridine. The procedure is described in details in articles [VIII]. The samples were kept at 70°C for 40 min and transferred to vials and then analyzed by GC. 1  $\mu\text{l}$  of the silylated sample was injected with an autosampler. The injection temperature was 260°C and the split ratio was 1:20. Hydrogen served as a carrier gas. The initial temperature of the column was 120°C (for 1 min), and the temperature was increased at a rate 6 K/min to 300°C (for 10 min). The peaks were identified by gas chromatography – mass spectrometry operating at the same GC (GC-MS, Hewlett Packard) conditions. The retention times of the main components were following:  $\alpha$ -conidendric acid - 25.7 min, HMR 1 - 26.3 min, HMR 2 - 26.4 min,  $\alpha$ -conidendrin - 26.6 min, oxoMAT - 26.9 min.

#### **2.4.4. Products of ethanol selective oxidation**

During the catalytic experiments, gas samples were analyzed periodically by online GC (gas chromatograph Tsvet-500; 30 m × 0.32 mm monolithic poly(divinylbenzene) capillary column; 170°C) with a flame-ionization detector for determination of ethanol, acetaldehyde, acetic acid, ethyl acetate, diethyl ether, ethylene and methane. For the determination of CO and CO<sub>2</sub>, they were preliminarily separated on a 1.5 m × 3 mm steel column filled with Porapak Q at 20°C followed by methanation. The selectivity to 1,1-diethoxyethane was estimated independently by analyzing the condensed outlet flow using GC-MS. The product analysis was performed in collaboration with the Laboratory of Selective Heterogeneous Oxidation at Boreskov Institute of Catalysis [VI].

## 3. Results and Discussion

### 3.1. Characterization of catalysts

#### 3.1.1. Support textural properties and Au particle size

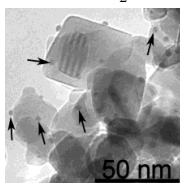
The support surface area was characterized by nitrogen adsorption measurements. The obtained data on the surface area measurements are presented in Table 1.

**Table 1.** Surface areas of the applied supports.

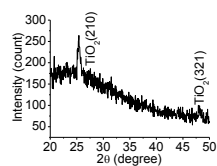
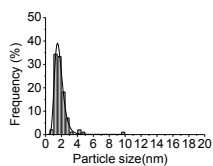
Support	BET surface area, m <sup>2</sup> /g
C (Sibunit)	450
Al <sub>2</sub> O <sub>3</sub> (A-201, UOP)	240
TiO <sub>2</sub> (Degussa AG, Aerolyst 7708)	45
SiO <sub>2</sub> (Merck)	520
Al <sub>2</sub> O <sub>3</sub> -I (Alfa-Aesar)	111
CeO <sub>2</sub> (Alfa-Aesar)	22
MgO(Alfa-Aesar)	37
ZrO <sub>2</sub> (Alfa-Aesar)	93
La <sub>2</sub> O <sub>3</sub> (Alfa-Aesar)	2
Al <sub>2</sub> O <sub>3</sub> -II	207
Ce(10)-Al	340
Ce(30)-Al	272
Ce(5)Zr(5)-Al	299
Ce(15)Zr(15)-Al	266
Al <sub>2</sub> O <sub>3</sub> -II	207

Gold particle sizes of the catalysts supported on the commercial and synthesized supports was determined by TEM and XRD measurements. Characterization of the data confirmed that gold particles were successfully deposited as nanoparticles in case of all supports utilized. Some of the obtained TEM images and XRD patterns are shown in Figure 1, where  $d$  is the average metal particle size. Catalysts Au/Al<sub>2</sub>O<sub>3</sub>–DPU and Au/Al<sub>2</sub>O<sub>3</sub>–DIE were prepared by DPU and DIE methods respectively.

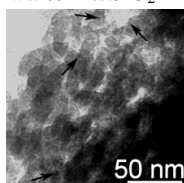
a) 2 wt.% Au/TiO<sub>2</sub>



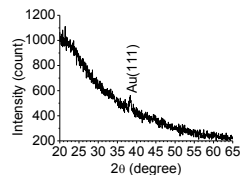
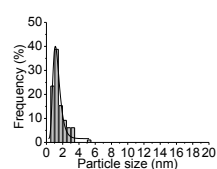
$d = 1.9 \pm 1.0$  nm



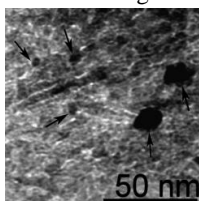
b) 2 wt. % Au/SiO<sub>2</sub>



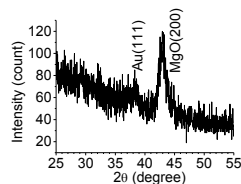
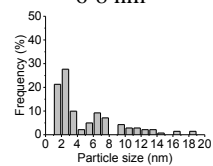
$d = 1.6 \pm 0.8$  nm



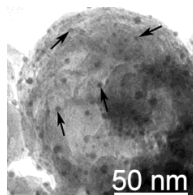
c) 2 wt. % Au/MgO



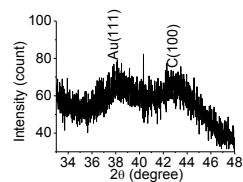
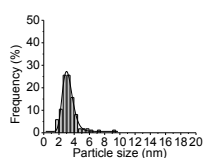
$d = 2-3$  nm and  
6-8 nm



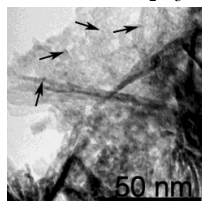
d) 2.5 wt. % Au/C



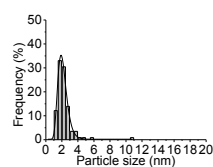
$d = 3.3 \pm 1.2$  nm



e) 2 wt. % Au/Al<sub>2</sub>O<sub>3</sub>-DIE

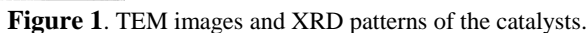


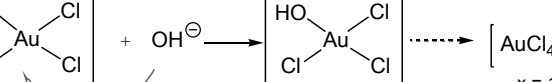
$d = 2.2 \pm 1.1$  nm



XRD is not reliable





1) 

Alumina (UOP, A-201) supported gold particle size was varied by changing the catalyst preparation parameters, such as the initial concentration of gold precursor, the washing agent, and the calcination temperature. A slight increase of the particle size with an increase on the

concentration of the precursor solution was observed. The effect of the calcination temperature on the particle size is revealed by Table 2.

**Table 2.** Properties of Au/Al<sub>2</sub>O<sub>3</sub> catalysts for arabinose oxidation, prepared by direct ion exchange (DIE) followed by ammonia and water (W) washing, and deposition-precipitation with urea (DPU) methods. The catalysts were calcined at 300, 400, 500, and 600°C, respectively. Numbers 1, 2, 3 denote the initial concentration of HAuCl<sub>4</sub>,  $5 \times 10^{-4}$ ,  $10^{-3}$ ,  $5 \times 10^{-3}$  M, correspondingly.

Catalyst	Metal loading, %	Average Au particle diameter, nm
DIE-300-1	1.5	1
DIE-300-2	1.6	1.2
DIE-300-3	2.0	1.3
DIE-400	2.2	2.5
DIE-500	2.2	3.4
DIE-600	2.2	3.7
DIE-300-W	2.1	2.9 and 28.1
DPU	2.0	2.3

In case of catalysts prepared by DIE the nature of the washing agent can modify the particle size of gold. The ion exchange (anionic in the present case due to the nature of the precursor) takes place during stirring the suspension of alumina in HAuCl<sub>4</sub> solution and keeping it at 70°C. The use of ammonia leads to partial or total elimination of chlorine species, being responsible for sintering. Therefore, smaller particles are expected for DIE-300-4 compared to DIE-300-W; this can be observed in Table 2. The catalyst DIE-300-W exhibited a bimodal distribution with the average sizes of 2.9 (between 1-5 nm) and 28.1 nm respectively. The particle diameter increased from 2.2 to 3.7 nm with increasing treatment temperature.

The values of the gold particle sizes on various oxides prepared at CNyN-UNAM and estimated from TEM images are presented in Tables 3. More than 200 particles were measured for each sample. The gold nanoparticles (NPs) found by TEM in the studied samples are characterized with a semispherical shape practically without any well detectable crystallographic planes. The average particle size depends on the nature of the supports used and varies for oxides in the range of 0.9-4.0 nm.

**Table 3.** Average particle sizes according to TEM measurements.

Support	Crystal size, nm		Gold particle size, nm
	Ceria	Alumina	
Al <sub>2</sub> O <sub>3</sub> -II	-	6.4	2.0
Ce(10)-Al	3.2	5.5	3.8
Ce(30)-Al	9.1	5.1	3.7
Ce(5)Zr(5)-Al	n.d.*	4.9	1.4
Ce(15)Zr(15)-Al	n.d.*	2.4	1.7
Al <sub>2</sub> O <sub>3</sub> -I	-	7.0	2.4
CeO <sub>2</sub>	43.0	-	2.2
MgO	-	-	4.0
ZrO <sub>2</sub>	-	-	1.8
La <sub>2</sub> O <sub>3</sub>	-	-	0.9

\* - not determined.

### 3.1.2. Acidity and basicity of the support

The presence of functional groups on the support surface plays an important role in the catalyst activity and selectivity. Therefore qualitative and quantitative analysis of the surface acid sites of the catalyst supports was performed. The nature of supports acid sites was studied by FTIR using pyridine as a probe molecule. Because of a good correlation between the acidities obtained by FTIR measurements and those obtained by TPD for a number of different acidic catalysts [79], the pyridine FTIR technique can be applied for a quantitative determination of acid sites. FTIR spectral interpretation was performed according to the commonly accepted procedure which attributes adsorption at about 1610 and 1450 cm<sup>-1</sup> to the Lewis acid sites, and peaks at 1545 and 1630 cm<sup>-1</sup> to pyridine adsorbed on the Brønsted acid sites. Brønsted acidity was not observed for any of the samples, while the number of Lewis acid sites was different.

Desorption of pyridine at 250°C, 350°C and 450°C was attributed to weak, medium and strong acid sites, respectively, according to [80]. The total concentration of acid sites was obtained at 250°C. Weak acid sites were defined as the difference between the concentration of acid sites obtained at 350°C and 250°C, the medium acid sites were calculated as a difference between concentrations at 450°C and 350°C, while the concentration of strong acid sites was detected at 450°C. The surface acid site distribution is given in Table 4.

In order to study the acidity and basicity changes during the catalyst preparation, alumina support free of gold was treated in the same way as during the catalyst preparation by DIE (consequent washing with ammonia and water followed by drying and calcination). The obtained sample denoted as Al<sub>2</sub>O<sub>3</sub>-DIE was analyzed by pyridine FTIR and CO<sub>2</sub>-TPD techniques. The amount of the Lewis acid sites on alumina decreased during the treatment according to the catalyst preparation procedure. At the same time, the basicity of alumina before and after the treatment was the same. Among the samples analyzed magnesia possesses the highest basicity.

**Table 4.** Acidities and basicities of the supports.

Support	Lewis Acid sites ( $\mu\text{mol/g}$ )				Basic sites ( $\mu\text{mol/g}$ )
	weak	medium	strong	total	
$\text{Al}_2\text{O}_3$ (A-201, UOP)				50	110
$\text{Al}_2\text{O}_3$ -DIE				10	110
$\text{SiO}_2$ (Merck)				0	
$\text{TiO}_2$ (Degussa AG, Aerolyst 7708)				150	84
MgO				0	250
$\text{Al}_2\text{O}_3$ -I (Alfa-Aesar)	15	10	0	25	
$\text{CeO}_2$ (Alfa-Aesar)	0	10	0	10	
$\text{ZrO}_2$ (Alfa-Aesar)	10	0	0	10	
$\text{La}_2\text{O}_3$ (Alfa-Aesar)	0	0	0		
MgO (Alfa-Aesar)	0	0	0		
$\text{Al}_2\text{O}_3$ -II	0	0	20	20	
Ce(10)-Al	10	10	0	20	
Ce(30)-Al	0	10	0	10	
Ce(5)Zr(5)-Al	10	10	0	20	
Ce(15)Zr(15)-Al	10	20	0	30	

Lanthanum oxide and magnesia have no acidity, which was expected due to their alkaline nature. Zirconia and ceria have shown a small amount of Lewis acid sites. Two kinds of aluminium oxides were applied, named further as  $\text{Al}_2\text{O}_3$ -I and  $\text{Al}_2\text{O}_3$ -II. The distribution of acid sites for these alumina samples is different; however, both are characterized with Lewis acid sites only.  $\text{Al}_2\text{O}_3$ -I has more weak and medium than strong acid sites, while  $\text{Al}_2\text{O}_3$ -II has strong acid sites only, although the total amount of Lewis acid sites is similar. The surface acidity of mixed oxides was compared to alumina ( $\text{Al}_2\text{O}_3$ -II). Addition of ceria to alumina decreases the strength of the surface Lewis acidity, which can be attributed to the increasing ceria loading and, thus, decreasing of the alumina fraction in the support. The presence of zirconia in the alumina-ceria mixed oxide results in the decrease of strong Lewis acid sites, while increasing the medium ones.

### 3.1.3. Electronic state of gold species

The electronic state of gold species was evaluated by XPS and UV-Vis techniques. The X-ray photoelectron (XPS) spectra of the Au 4f core level of Au/Al<sub>2</sub>O<sub>3</sub> catalysts show only one band corresponding to Au<sup>0</sup>. However, in the case of Au/TiO<sub>2</sub> and Au/SiO<sub>2</sub>, the contribution of two metal states was detected: Au<sup>0</sup> and Au<sup>δ+</sup>. These observations could be explained by two phenomena: an electron transfer from the support towards the gold particles [81, 82], or a dominant effect of the atoms at low coordinated sites as proposed by Claus and co-workers [83]. The first one could be applied only to the titania-supported catalyst, since silica demonstrates weak interactions with the noble metal clusters [84]. The effect of low coordinated atoms could be detected in case of both carriers, silica and titania, since the gold particle size is lower than 2 nm.

Typical XPS spectra of gold supported on ceria and Ce(30)-Al mixed oxide are presented in Figure 2. The Au 4f spectra with two spin-orbit components Au 4f<sub>7/2</sub> and Au 4f<sub>5/2</sub> separated by 3.67 eV, exhibit two doublets attributed to different gold species only in the case of the Au/CeO<sub>2</sub>, where curve fitting of Au 4f spectra indicated the following Au 4f<sub>7/2</sub> components at a binding energy values of ~83.8 and 84.5 eV corresponding to Au<sup>0</sup> and Au<sup>+</sup> species, respectively, according to [85-87]. Thus, according to XPS data, some portion of Au<sup>+</sup> cations was still present in the reduced Au/CeO<sub>2</sub> sample. The high full width at half maximum (FWHM) value for Au<sup>+</sup> cations in the reduced Au/CeO<sub>2</sub> sample compared with the FWHM value for Au<sup>0</sup> implied that these cations were formed within the thin layer probably located at the gold-ceria interface as it was also mentioned in ref. [88].

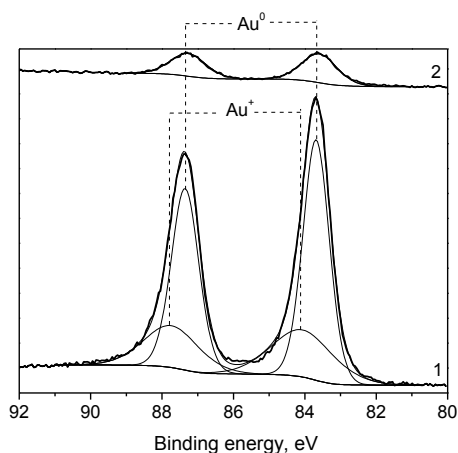


**Figure 2.** Au 4f XPS spectra for samples: 1 – Au/CeO<sub>2</sub> and 2 – Au/Ce(30)-Al.

Gold catalysts studied in the current work are characterized by the presence of Au<sup>0</sup> species only, except for titania, silica and ceria supported catalysts. The absence of Au<sup>+</sup> species in the catalysts based on mixed oxides could be due to a lower content of ceria in mixed oxides. Dilution of ceria with alumina may decrease the portion of gold cations, which could be

formed due to a contact of gold with ceria by several times because of the gold species location on mixed oxides both on ceria and alumina surface sites.

UV-Visible DR spectra of gold samples supported on zeolites, commercial oxides and nanostructured mixed oxides prepared by sol-gel are discussed in detail in article [IX]. The spectra of gold supported on different oxides are characterized by an adsorption band at around 520-580 nm, which could be assigned to the peak of plasmon resonance due to the presence of metallic gold particles as proposed in [89-92].

The position of the plasmon peak depends on both gold particle size and the dielectric function of the media [93]. As it is discussed in detail in ref. [94], the position of the plasmon peak for gold NPs supported on nanostructured Ce-Al-O mixed oxides depends mainly on the dielectric properties of surrounding media, when gold NPs may be stabilized both on alumina and ceria surface sites.

### 3.2. Isomerization of linoleic acid [III]

Gold catalysts supported on Al<sub>2</sub>O<sub>3</sub> (A-201, UOP), TiO<sub>2</sub>, SiO<sub>2</sub>, MgO, C (Sibunit) were tested in the linoleic acid isomerization, demonstrating different behaviors. The selectivity of synthesized catalysts towards hydrogenation and conjugation towards desired products were investigated. The most selective catalysts among the investigated ones were Au supported on SiO<sub>2</sub> and C [III]. Moreover, in order to reveal the influence of the functional groups on the carbon surface, carbon support (C<sub>ox</sub>) was preoxidized by aqueous HNO<sub>3</sub> (5 wt. %) prior to the catalyst synthesis.

Gold supported on preoxidized carbon 1 wt. % Au/C<sub>ox</sub> provided the highest conversion of linoleic acid and the highest yield of hydrogenation products (Table 5), possessing the lowest metal loading among the catalysts tested. However, the highest selectivity towards the conjugation was observed over the non-oxidized carbon supported gold catalyst.

**Table 5.** The properties of gold catalysts in the linoleic acid isomerization. Reaction time 4 h. X = conversion; S<sub>i</sub> = selectivity. Hydr. = hydrogenation.  $\Sigma$ CLA = sum of CLAs.

Sample	X, %	S <sub>cis-</sub> 9,trans-11, %	S <sub>trans-</sub> 10,cis-12, %	S <sub>trans-</sub> 9,trans-12, %	S <sub>Hydr.</sub> , %	$\Sigma$ CLA, %	Hydr./ $\Sigma$ CLA
Au/C	4	32	23	45	0	100	0
Au/C <sub>ox</sub>	60	2	0	6	90	8	11
Au/SiO <sub>2</sub>	4	34	0	40	26	74	0.4

Despite the fact that three different samples of gold catalysts have approximately the same gold particle sizes, the behaviors of these catalysts in linoleic isomerization were different. It can be thus concluded that chemical properties of the support play an important role. Different catalytic behaviors of gold catalysts can be most likely related to the difference of their surface chemistry. The presence of acidic groups on the support surface in the case of oxidized carbon and silica results in the formation of hydrogenation products in linoleic acid isomerization due to the higher acidity of the supports compared to non-oxidized carbon

resulting in the protons donation. Although silica and non-oxidized carbon supported gold catalysts show the same activity at the same time, there are no hydrogenation products were obtained in the case of the carbon supported catalyst. This can be attributed to the mechanism of the reaction involving the proton transfer and the subsequent hydride transfer mechanism leading to hydrogenation [95, 96].

### 3.3. Selective oxidation reactions

Since oxidative dehydrogenation has been a generally accepted mechanism for the selective oxidation of alcohols, both terms “selective oxidation” and “oxidative dehydrogenation” were applied to describe the oxygen-assisted reactions studied in the current work.

#### 3.3.1. Gas-phase selective oxidation of ethanol [IV-VI]

The catalytic activity and selectivity of titania, alumina (A-201, UOP) and silica supported gold catalysts were compared. The profile of the ethanol conversion contains the low temperature peak with an upper bound of 60% at 120°C. The catalytic behavior of Au/TiO<sub>2</sub> is different from Au/Al<sub>2</sub>O<sub>3</sub> and Au/SiO<sub>2</sub> catalysts (Figure 3). Alumina and silica supported catalysts induce a usual, steadily rise of ethanol conversion with increasing temperature, which becomes significant at temperatures exceeding 200°C.

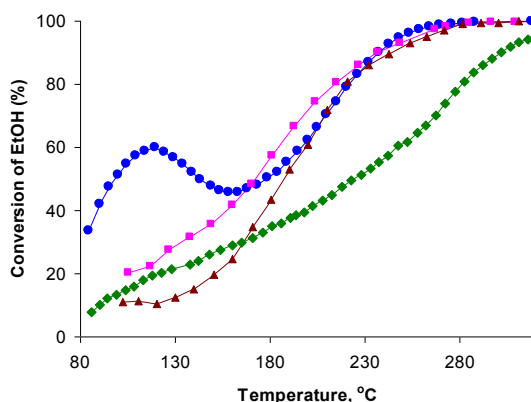


**Figure 3.** Ethanol conversion over TiO<sub>2</sub> (▲), 2 wt.% Au/TiO<sub>2</sub> (●), 2 wt.% Au/Al<sub>2</sub>O<sub>3</sub> (■) and 1 wt.% Au/SiO<sub>2</sub> (◆). Gas mixture: 2 vol.% EtOH, 18 vol.% O<sub>2</sub> and He balance, GHSV = 3600 h<sup>-1</sup>.

The catalytic performance of 2 wt. % Au/TiO<sub>2</sub> in a single pass flow reactor system is displayed in Figure 4. The main reaction product was acetaldehyde. At higher temperature the lack of mass balance completion is mostly associated with the production of diethyl ether and ethylene. The oxidation of alcohols over gold catalysts at temperatures lower than 150°C is typically performed in the liquid phase [97-100]. However, the solvent-free reaction performance is more attractive from an industrial point of view. The reaction temperatures currently reported for the selective gas-phase oxidation over various Au catalysts are generally above 200°C, which leads to a high energy consumption and catalyst deactivation.

Therefore, the low temperature activity of Au/TiO<sub>2</sub> catalysts in the gas-phase ethanol oxidation observed in article [IV] seems to be promising for practical applications.

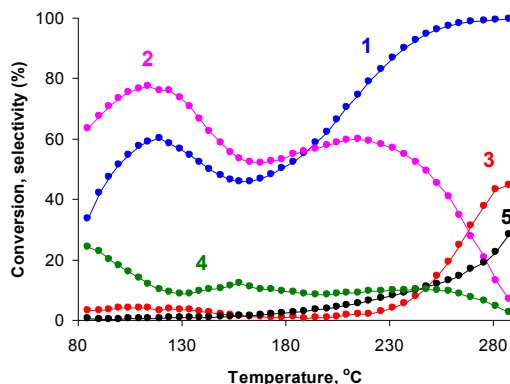
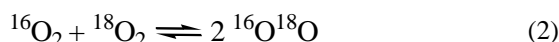
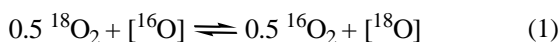


**Figure 4.** Catalytic performance of the 2 wt. % Au/TiO<sub>2</sub> catalyst as a function of the reaction temperature: conversion of ethanol (1) and selectivities towards acetaldehyde (2), acetic acid (3), ethyl acetate (4), and CO + CO<sub>2</sub> (5).

In order to explain the unusual ‘double peak’ catalytic activity of Au/TiO<sub>2</sub> in the gas-phase selective oxidation of ethanol, the formation of specific active oxygen form (catalytic sites) on the Au/TiO<sub>2</sub> surface under mild reaction conditions was proposed. The O<sub>2</sub> isotope exchange technique (OIE) was applied to estimate the relative activity of the surface oxygen species [IV]. Generally, in a heterophase system comprising molecular dioxygen (O<sub>2</sub>) in the gas phase and oxygen on the surface of a solid (O), two isotope exchange reactions take place: 1) the hetero-exchange reaction (Eq.1), which is conveniently monitored by a fraction of the <sup>18</sup>O isotope in the gas phase; and 2) the homo-exchange reaction (Eq. 2). The low-temperature activity of a catalyst in an oxygen homoexchange can indicate the involvement of active surface oxygen species.



Ethanol was shown to undergo dehydrogenation and dehydration over supported gold catalysts. The superior dehydrogenation activity of the Au/TiO<sub>2</sub> catalyst compared to the Au/SiO<sub>2</sub> and Au/Al<sub>2</sub>O<sub>3</sub> catalysts was observed. Moreover, the Au/TiO<sub>2</sub> catalyst was active in the consumption of hydrogen at 150°C, followed by formation of water at increasing temperature due to interactions with the surface oxygen. In contrast to a non-treated catalyst, the sample treated in hydrogen was able to catalyze the oxygen isotope homoexchange at quite low temperatures. A similar but notably less intensive isotope exchange was induced by Au/Al<sub>2</sub>O<sub>3</sub>, whereas Au/SiO<sub>2</sub> did not evoke this reaction at all.

A possible explanation for the obtained results is the formation of an active oxygen species on the Au/TiO<sub>2</sub> and Au/Al<sub>2</sub>O<sub>3</sub> surfaces after the treatment of the samples with H<sub>2</sub>. These species are able to catalyze the oxygen isotope homoexchange reaction. They might be also



responsible for the low temperature oxidation of ethanol over Au/TiO<sub>2</sub> in the temperature region of 80-150°C.

The nature of these oxygen species is not yet clear. It may be the surface O<sup>-</sup> anion radical as suggested both for  $\alpha$ -oxygen in Fe-ZSM5 zeolite [101] and for photo-oxidation over TiO<sub>2</sub> [102]. Another possibility is formation of surface O<sub>2</sub><sup>-</sup> superoxide ions. In case of propylene epoxidation, the commonly accepted mechanism supposes the formation of hydrogen peroxide and hydroperoxo species as key intermediates. Therefore, one also can assume the involvement of peroxides in the ethanol oxidation over Au/TiO<sub>2</sub>.

The thermal stability of the surface active species was evaluated based on the temperature dependence of the oxygen isotope homoexchange rate. The active oxygen species on the Au/Al<sub>2</sub>O<sub>3</sub> surface are much less stable and cannot exist at all in the temperature range of 80 to 150°C. This may explain the difference in the catalytic activity of gold supported on TiO<sub>2</sub> and Al<sub>2</sub>O<sub>3</sub> in the ethanol oxidation.

### **3.3.2. Structure sensitivity of L-arabinose selective oxidation [VII]**

The different particle sizes presented for the studied catalyst allowed a systematic evaluation of the influence of the average particle diameter on the catalytic activity. An optimal particle size giving the highest activity was achieved over the mean gold particles of 2.3 nm (Figure 5).

It is well known that the activity of a supported gold catalyst is dependent on the particle size (structure sensitivity) and the nature of the support. When gold is deposited on an inert support such as carbon, the observed catalytic activity is only related to the properties of gold. When the support is a metal oxide, the scenario is different, because of the interactions between the support and the noble metal, which cannot be neglected even for such supports as alumina. Analysis of the structure sensitivity in the present work follows a classical approach based on the average values, obtained by TEM. The activity values are not related to the particle morphology or the particle size distribution. The calculations of the gold dispersion were based on the assumption that gold particles are cubo-octahedral, even though particles around 1 nm have also icosahedral structures and above 1 nm decahedral crystals appear. By analogy with the mechanism proposed by Claus for the oxidation of D-glucose [103], it is reasonable to assume that L-arabinose is adsorbed on gold atoms via the carbonyl group. Below the size of 2 nm, Au particles are monolayers and all the atoms are in contact with the support, whereas for larger particles the number of these sites decreases. The catalysts prepared by DPU with an average diameter of 2.3 nm had the maximum number of active sites for the adsorption of arabinose and activation of oxygen. Since low-coordinated gold atoms, having mainly edges and corners, demonstrated catalytic activity lower than particles larger than 2 nm, catalysts activity was attributed to the presence of faces on the Au particles surface, where the reaction takes place. Therefore, the volcano-type relationship (Figure 5) between the activity and the gold particle size can be explained by the population of the active sites for the adsorption of arabinose; dehydrogenation step and oxygen activation.

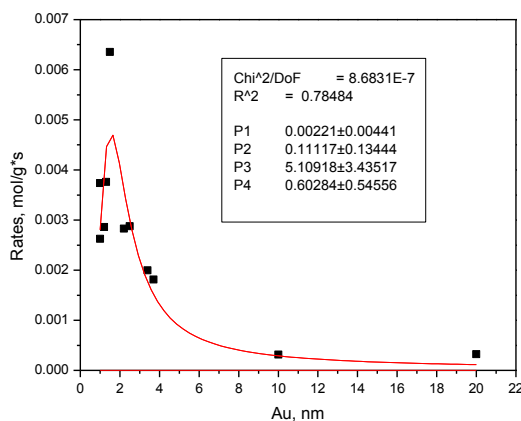


**Figure 5.** The dependence of the initial rates at L-arabinose oxidation on the particle size of Au/Al<sub>2</sub>O<sub>3</sub>.

An expression for a Langmuir-Hinshelwood mechanism was obtained in [104], which could be written for arabinose oxidation in the following way:

$$V(r) = \frac{k' K_A C_A K_{O_2} C_{O_2} e^{2\alpha\Delta\delta / RT} r}{(1 + K_A C_A e^{\Delta\delta / RT} + K_{O_2} C_{O_2} e^{\Delta\delta / RT})^2} \quad (3)$$

where  $V$  is the catalyst activity,  $C_A$ ,  $C_{O_2}$ , is the concentration of arabinose and dissolved oxygen, respectively,  $k$  is the rate constant,  $K_A$  and  $K_{O_2}$  – adsorption coefficients for arabinose and oxygen respectively,  $\Delta\delta$  - a proportionality coefficient between the chemical potential increment for nanoclusters compared to extended surfaces and the cluster radius  $r$ ,  $\alpha$  - Polanyi parameter (typically close to 0.5).

This is a simplified kinetic expression, since it does not include the dependence of the rate on pH. Moreover, adsorption of oxygen might not only be molecular, but also dissociative. However, this difference cannot be revealed using the available experimental data on the cluster size effect, since the experiments were conducted at a constant oxygen pressure. A kinetic equation somewhat similar to (3) was utilized previously for a quantitative description of lactose oxidation on gold catalysts. Eq. (3) could be simplified, leading to a four-parameter dependence

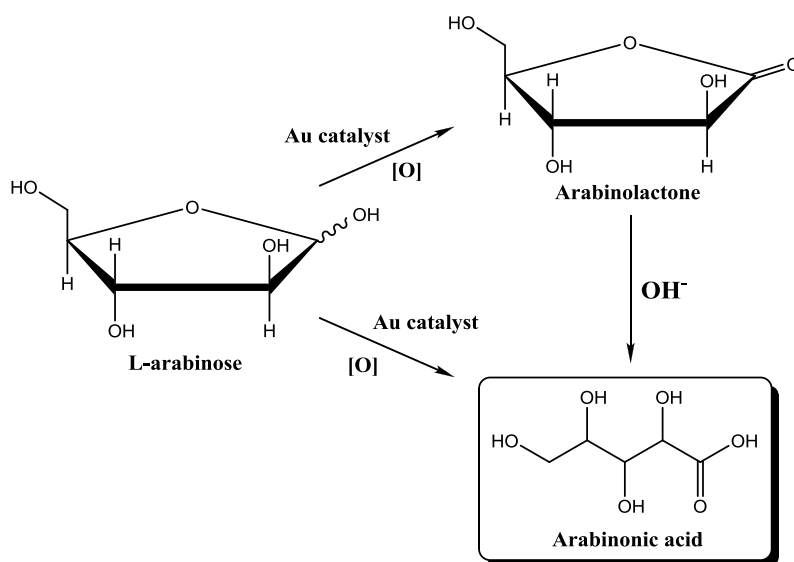
$$V(r) = \frac{p_1 e^{2p_4 p_3 / d}}{(1 + p_2 e^{p_3 / d})^2} \frac{1}{d} \quad (4)$$

where  $d$  is the diameter of clusters, and:

$$p_1 = 2k' K_A C_A K_{O_2} C_{O_2} \quad p_2 = K_A C_A + K_{O_2} C_{O_2}$$

$$p_3 = 2\Delta\delta / RT \quad p_4 = \alpha$$

Results of the calculations along with the values of the parameters are shown in Figure 5, confirming a good correspondence between the calculations and the model. The selectivity towards arabinolactone and arabinonic acid (see Scheme 5) showed the dependence only on the conversion, but was not influenced by the particle size, most probably, because both reactions take place on the same type of sites. The increase of the availability of these sites results in an increase of both reaction rates.



**Scheme 5.** The reaction pathway of L-arabinose oxidation over gold catalysts.

According to the reaction mechanism proposed by Kusema et al. [105], the oxidation of sugars proceeds through an oxidative dehydrogenation, where arabinolactone is an intermediate, followed by the oxidation of adsorbed hydrogen with dissociatively adsorbed oxygen.

### 3.3.3. Liquid-phase oxidation of the lignan hydroxymatairesinol [VIII-XI]

#### 3.3.3.1. Effect of the solvent and the reaction atmosphere

Since the lignan HMR is poorly soluble in water and hydrocarbons, but well soluble in alcohols, the reaction was performed in different alcohols and their mixtures with water. In order to avoid competitive oxidation of HMR and alcohols over the gold catalyst, the reaction was also performed using 1,4-dioxane and tetrahydrofuran (THF) and their mixtures with water as a solvent [VIII]. Gold catalysts were not active in this reaction, when ethanol, 2-propanol, 1-butanol, 2-pentanol were used as solvents. However, application of alcohol and water mixtures as a solvent results in the formation of the desired product – oxoMAT. The formation of oxoMAT was also observed in solvents different from alcohols, e.g. 1,4-dioxane and tetrahydrofuran (THF) and their mixtures with water.

The screened gold catalysts were not active in the oxoMAT synthesis, when pure alcohols were applied as solvents. However, utilization of alcohol with water mixtures results in oxoMAT formation due to the HMR oxidation [VIII]. These changes could be related to the activity of gold catalysts in the alcohol oxidation, thus, the catalysts interact with the alcohol in the solvent rather than with HMR. Alcohol can be oxidized over gold, leading to compounds, which poison gold catalysts, as for example, acetone via 2-propanol oxidation or other aldehydes and carboxylic acids generated from the corresponding alcohols. Thus, when an alcohol-water mixture was applied, gold catalysts became active in the oxoMAT synthesis due to minor alcohol oxidation. Moreover, the catalytic activity is increasing with an increasing water content in the reaction mixture. The highest activity and selectivity were reached applying 2 and 5 vol. % 2-propanol in water as a solvent. The role of water could be related to three phenomena: first, suppression of the possible deactivation described above, due to organic solvent interactions with the catalyst surface; second, activation of adsorbed oxygen by adsorbed water due to the formation of the hydroperoxyl-like intermediate species ( $\text{OOH}$ ) followed by their decomposition and release of  $\text{O}^*$  and  $\text{H}_2\text{O}$ , and third, the hydrolysis of the metal oxide support, followed by the formation of the surface OH-groups, enhancing the adsorption of HMR on the catalyst surface in the geometry suitable for a further dehydrogenation.

In contrast to previously applied Pd catalysts, gold demonstrated higher activity in the presence of oxygen than under the same reaction conditions in its absence [VIII]. Moreover, gold catalysts demonstrated a complete selectivity to the desired oxoMAT compared to a selectivity of 70% obtained over Pd catalysts. It was also reported, that gold catalysts have a catalytic activity in the alcohol oxidation in the absence of oxygen [106]. However, the presence of oxygen leads to the removal of adsorbed hydrogen atoms by co-adsorbed oxygen, thus, increasing the reaction rate. A typical concentration on time dependences are presented in Figure 6.

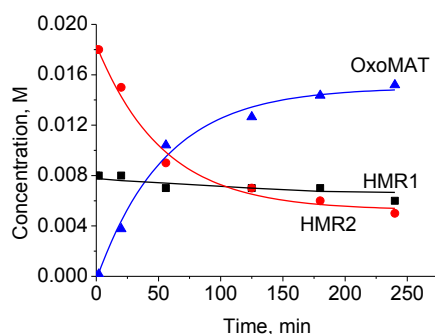


**Figure 6.** The oxidation of HMR in 2 vol. % 2-propanol in water (250mg of 2 wt. %  $\text{Au}/\text{Al}_2\text{O}_3$ –DIE catalyst at  $70^\circ\text{C}$  under the flow of synthetic air).

## 3.3.3.2. Effect of the catalyst support and active phase

The tested gold catalysts have shown different activities toward oxidation/dehydrogenation of HMR [VIII-IX]. Among them the most active catalyst was gold supported on alumina (Figure 7).

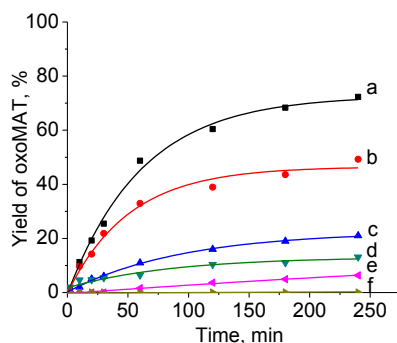
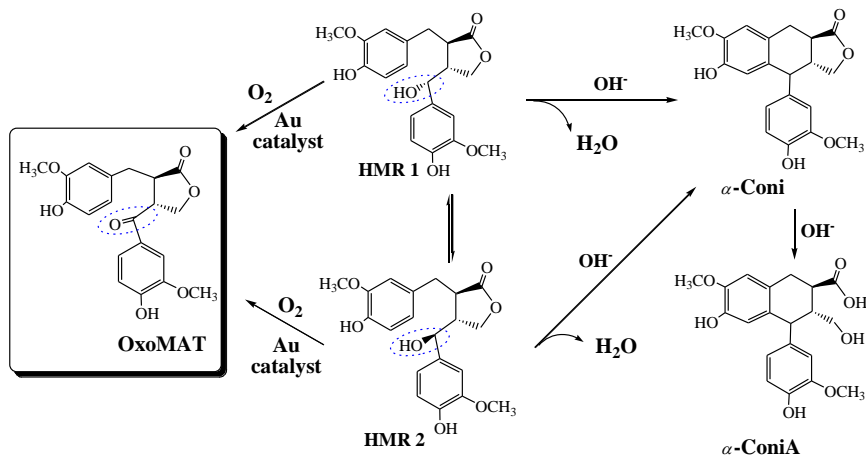
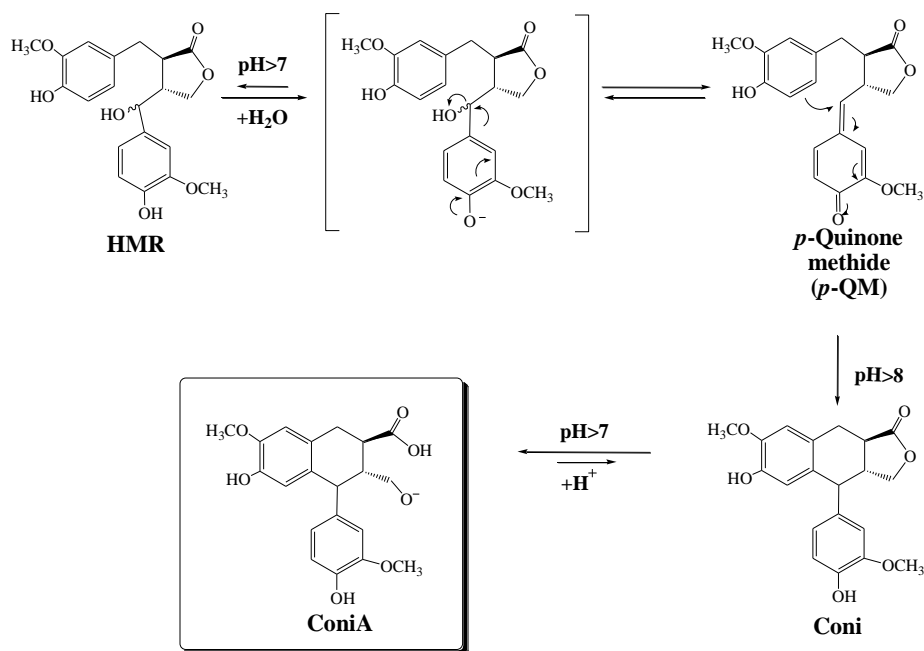


**Figure 7.** The oxoMAT yield as a function of time at 70°C using 2 vol. % 2-propanol in water as a solvent in air flow over 250 mg catalysts: a) Au/Al<sub>2</sub>O<sub>3</sub> – DIE; b) Au/Al<sub>2</sub>O<sub>3</sub> – DPU; c) Au/TiO<sub>2</sub>; d) Au/SiO<sub>2</sub>; e) Au/C; f) Au/MgO.

In the case of Au/MgO catalysts, HMR was transformed into other lignans: conidendrin (Coni) and conidendric acid (ConiA) (see Scheme 6) by HMR dehydration, which was followed by cyclisation. This behavior is related to the basicity of magnesia, as ConiA is normally formed with an increasing pH value of the solution (see Scheme 7).



**Scheme 6.** The reaction pathway of the lignan hydroxymatairesinol (HMR) transformation over gold catalysts under aerobic conditions.



**Scheme 7.** Transformations of the lignan hydroxymatairesinol (HMR) to lignans condendrin (Coni) and condendric acid (ConiA) in alkaline solution (pH 7-10).

Since Au/Al<sub>2</sub>O<sub>3</sub> catalysts have demonstrated the highest activity and selectivity towards oxoMAT synthesis, HMR oxidation was further studied over series of gold catalysts supported on alumina-ceria-zirconia mixed oxides and gold supported on different alumina supports. However, addition of ceria and zirconia to alumina did not improve the catalyst performance (Figure 8). Among the tested alumina catalysts, the activity increased with the increase of the support pore size.

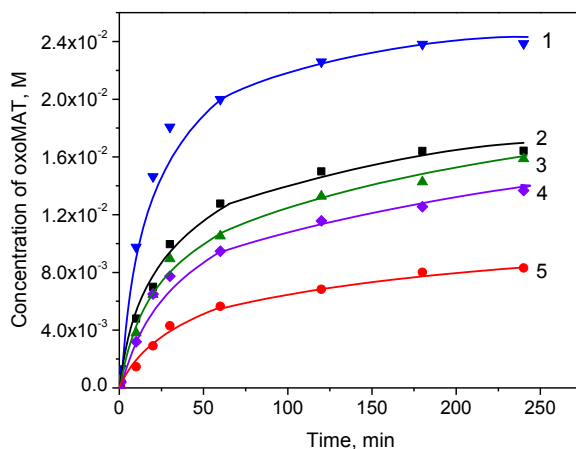
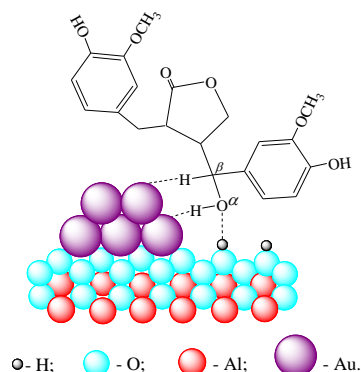


**Figure 8.** The dependence of the oxoMAT concentration on time over 3 wt. % Au catalysts supported on oxides prepared by sol-gel: 1 = Au/Al<sub>2</sub>O<sub>3</sub>-II; 2 = Au/Ce(5)Zr(5)-Al, 3 = Au/Ce(10)-Al; 4 = Au/Ce(15)Zr(15)-Al; 5 = Au/Ce(30)-Al. Conditions:  $m_{\text{cat}}=0.200$  mg, under synthetic air flow, at 70°C.

In general, the activity of supported gold catalysts increased with an increasing Lewis acidity of the corresponding supports. This phenomenon was attributed to the increasing amount of the surface OH-groups, formed via support hydrolysis at the reaction conditions, which is important for a suitable adsorption of HMR on the catalyst. The proposed adsorption mode is given in Figure 9. According to this model, the HMR hydroxyl group is coordinated by the oxygen atom to the surface hydroxyl-group, while the hydrogen removal is performed on the gold particle surface located at the distance corresponding to the molecule geometry.

**Figure 9.** Proposed scheme of the HMR molecule adsorption on Au/Al<sub>2</sub>O<sub>3</sub>.



In order to investigate the influence of bimetallic interactions and support properties, gold, gold-palladium, and palladium catalysts were tested in the lignan HMR selective oxidation [IX]. Their activity and obtained products yields were compared to those of the corresponding

supports. All supports applied *per se* were not active in the oxoMAT synthesis, while supported gold catalysts showed different activities in the HMR transformation. However, the most important difference in the catalytic behavior was the selectivity towards various products. It was observed, that the selectivity of the reaction is dependent on the support surface functional groups and the activity of the gold particles. If the support activity is the dominating factor, substrate side reactions, i.e. isomerization HMR 2 to HMR 1, and formation of Coni and ConiA, predominantly occurred. Otherwise, the selectivity is shifted towards the oxidation of HMR. Bimetallic Au-Pd catalysts demonstrated results similar to those obtained over corresponding monometallic Au catalysts.

#### 3.3.3.3. *Catalyst deactivation and regeneration*

Deactivation of gold catalysts during the HMR oxidation was observed. The reasons for decreasing the catalyst activity and a possibility to regenerate the spent catalyst were studied in article [X]. The reasons of the catalyst deactivation could be poisoning by reagents and solvent impurities, catalyst leaching, gold particles sintering and catalyst surface reconstruction, or strong adsorption of the reaction and side-reaction products, which can form oligomeric or polymeric structures.

The biomass-derived lignan HMR contains inorganic impurities, although no poisoning elements, such as Cl, S, P, etc., were detected. Organic impurities of HMR are lignans Coni and ConiA, which can be adsorbed on the catalyst and decrease the activity. The influence of the product oxoMAT was also investigated. It was discovered, that the catalyst activity was decreasing during the product formation. However, the experiments with a fresh catalyst in the presence of the product demonstrated an increase of the catalyst activity in each subsequent experiment. Nevertheless, the presence of adsorbed organic species was confirmed by TPO, where their combustion was observed at increasing temperature. Thus, the adsorption of oxoMAT could also be a reason for the catalyst deactivation, while the impact of that is moderate. Potential changes of the catalyst surface area, Au particle size and the metal loading were also elucidated. The leaching of the active phase was suggested to be the most important, although the observed changes were within a measurement error.

Since the catalyst deactivation is most likely could be the adsorption of organic compounds adsorption, attempts to regenerate the catalyst by extraction and calcination were made. Calcination was found to be the most efficient method (Figure 10), although the calcination temperature should not exceed 500-600°C to avoid catalyst sintering and support changes.



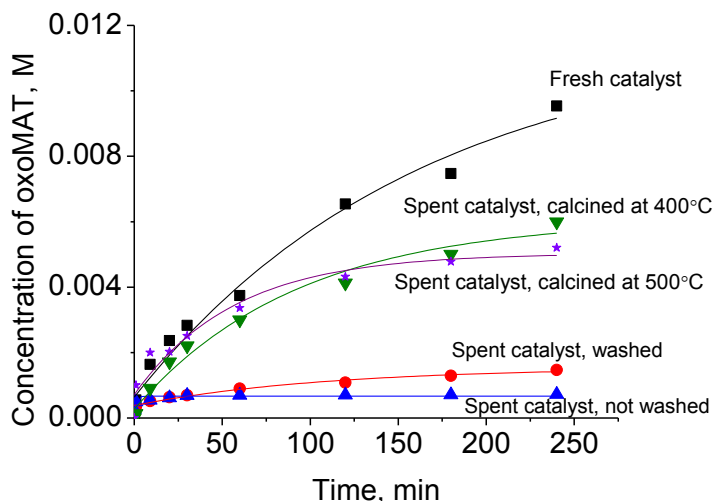


**Figure 10.** The oxoMAT concentration profile during the selective oxidation of HMR over 2 wt. % Au/Al<sub>2</sub>O<sub>3</sub>: fresh, spent/calcined, spent/washed and spent/non-washed catalysts.

#### 3.3.3.4. Reaction kinetics

The kinetic regularities of the aerobic selective HMR oxidation over gold catalysts were revealed. The reaction kinetics clearly shows a non-zero order behavior with respect to the substrates HMR 1 and HMR 2. Linearization of kinetic data in the logarithmic coordinates gave the reaction order values about  $0.417 \pm 0.050$  and  $0.287 \pm 0.075$  for HMR 1 and HMR 2 isomers, respectively (Figure 11), while an approximately first-order ( $0.800 \pm 0.080$ ) with respect to the catalyst was obtained. The possible deviation from the first order behavior could be explained by the retardation of the reaction rate with the product oxoMAT. This results in the presence of the oxoMAT concentration in the denominator of the reaction rate equation, which also depends on the HMR concentration. The observed reaction inhibition could be related not only to the product adsorption, but also to adsorption on the catalyst active sites of the lignan Coni present in the substrate.

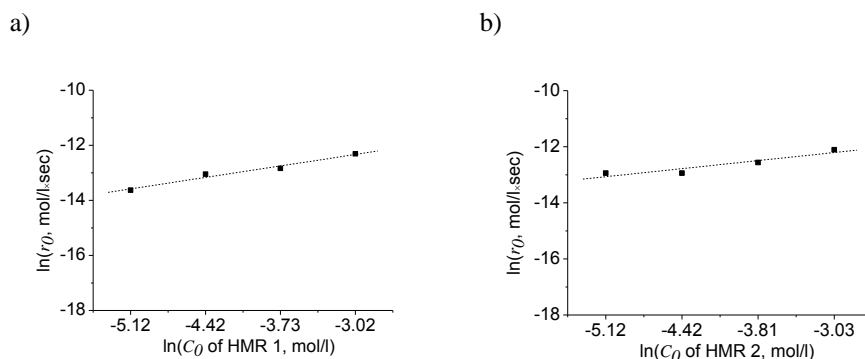


**Figure 11.** The logarithm of the initial reaction rate ( $r_0$ ) of a) HMR 1; b) HMR 2 as a function of the concentration ( $C_0$ ) logarithm at the corresponding isomers.

When the influence of oxygen partial pressure was studied, the reaction rate was found to be independent on the oxygen amount following, thus, zero-order behaviour. The role of oxygen in the reactions of selective oxidation over gold catalysts was studied in a number of papers, where activated by catalyst oxygen was found to: a) interact with water, forming oxidizing active species [107, 108]; b) act as a Brønsted basic site, enhancing O-H bond cleavage [109] as well as  $\beta$ -H removal which resulted in formation of corresponding aldehydes/ketones [106]; c) scavenge the electrons deposited on gold during the reaction mechanism [110]. In the later work, the reaction rate of ethanol oxidation is increasing up to oxygen concentration of 10 vol. %, thereafter remaining constant.  $\beta$ -H removal is considered to be the limiting step of the oxidative dehydrogenation, while it is catalyzed by adsorbed oxygen. In case of HMR oxidation reaction, the reaction rate is independent on oxygen partial pressure in the range of 5 to 49 vol. % of oxygen (see Figure 12). At the same time, as was shown in article [VIII], in anaerobic conditions reaction rate is dramatically decreased.

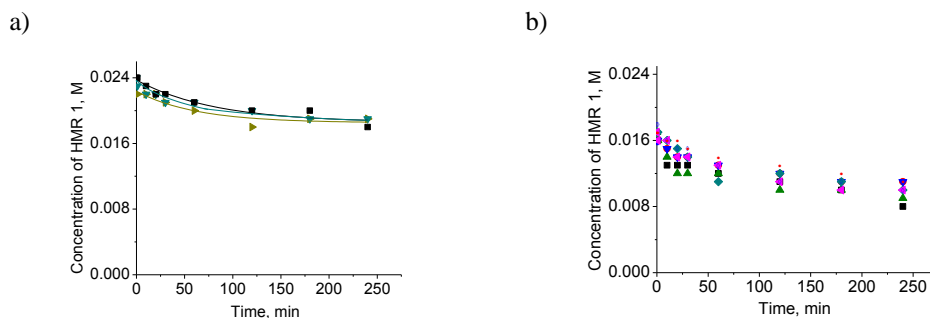
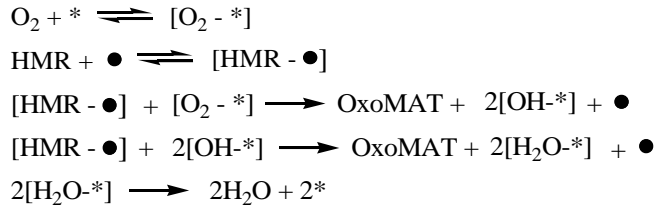


**Figure 12.** Concentration vs. time dependency of : (a) HMR 1; (b) HMR 2 over 250 mg 2 wt. % Au/Al<sub>2</sub>O<sub>3</sub> catalyst at 70°C, under different oxygen content: (●) 5.5 %, (◇) 8.6 %; (►) 12 %; (▲) 24 %; (▼) 32 %; (■) 39 %; (◄) 44 %; (●) 49 %.

The role of oxygen in the reaction mechanism of aerobic oxidation of HMR will be discussed below (see Section 3.3.3.6). The apparent zero-order with respect to oxygen could be explained by following assumptions, similar to the case studied in Ref. [111]. Oxygen and HMR molecules do not compete for the adsorption sites. The adsorbed oxygen is in equilibrium with oxygen dissolved in the liquid phase. Thus, the reaction rate does not depend on the adsorbed oxygen concentration.

Both isomers can be oxidized to form oxoMAT, therefore, transformation of each isomer should be included in the kinetic model. The reaction steps are shown below, where HMR stands for both, HMR 1 and HMR 2, isomers.



where \* - is the catalyst active site, available for oxygen adsorption,  $\bullet$  - is the catalyst site, available for HMR adsorption.

The reaction rates for each isomer oxidation can be calculated according to the following equations:

$$r_1 = k_1 \times C_{\text{HMR1}} \times p(\text{O}_2) \quad (4)$$

$$r_2 = k_2 \times C_{\text{HMR2}} \times p(\text{O}_2) \quad (5)$$

where  $k_1$  and  $k_2$  are lumped reaction rate constants, containing also adsorption terms,  $C_{\text{HMR1}}$  and  $C_{\text{HMR2}}$  are the concentration of HMR 1 and HMR 2, respectively;  $p(\text{O}_2)$  is the partial pressure of dissolved oxygen.

Since the transformation of HMR 2 to HMR 1 was not detected in the cases studied, it was not included in the kinetic model. The generation rate of oxoMAT is given by

$$\frac{dC_{\text{oxoMAT}}}{dt} = (r_1 + r_2) \frac{m_{\text{cat}}}{V} \quad (6)$$

where  $m_{\text{cat}}$  is the catalyst mass,  $V$  is the liquid volume.

The difference in the reaction rates in two cases, when either isolated isomers or a mixture of them was used, can be explained by a competitive adsorption of two isomers, thus, affecting the reactivity of each other. The values of the rate and adsorption constants were estimated through numerical data fitting using a parameter estimation software. An example of the modelling results is presented in Figure 13.

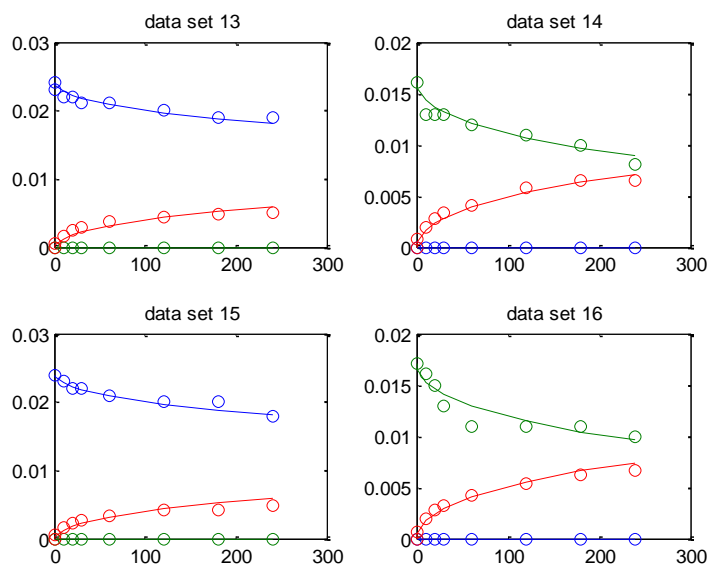


**Figure 13.** The comparison of experimental data (solid line) and simulation results (open symbols). The oxidation reactions were performed with isolated HMR isomers. Compounds: HMR 1 (green), HMR 2 (blue) and oxoMAT (red).

### 3.3.3.5. Structure sensitivity

The catalytic activity of Au/Al<sub>2</sub>O<sub>3</sub> catalysts with different particle sizes (1.9-10 nm) was tested for the HMR oxidation. The relationship of the catalyst activity with the gold cluster size has a volcano-shape dependence with a maximum at 3.2 nm (Figure 14). The result is similar to the one obtained for L-arabinose oxidation, where the most active catalyst has an average Au particle size of *ca.* 2 nm. The difference in the geometry and molecule size of the substrates could be a reason for the different optimum cluster sizes. Thus, larger HMR molecules require a larger Au cluster size suitable for the adsorption. The calculated dependence of TOF on the Au particle size is presented in Figure 15. Lower values of TOF in the case of the catalysts with an average size 1.9-3 nm, compared to those obtained at 3.2-10 nm can be attributed to two phenomena: first, small particles (1.9 nm) can contain a fraction of positively charged gold (Au<sup>δ+</sup>), second, as mentioned above, the size of such small particles is not suitable to accommodate HMR.

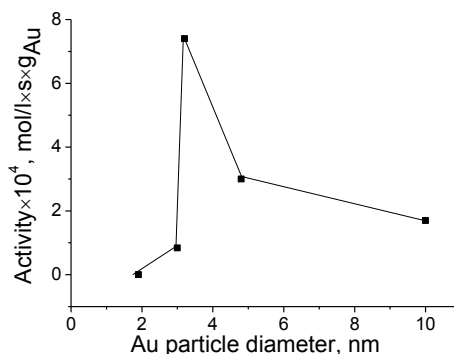


**Figure 14.** The dependence of the initial rate in the selective oxidation of the lignan hydroxymatairesinol (HMR) on Au particle size of Au/Al<sub>2</sub>O<sub>3</sub>.

Gold particles of 3.2-10 nm have similar values of TOF, which is an evidence for the independence of the reaction performance on the type of gold active sites. This result can be explained as well in terms of the HMR adsorption mode. As was proposed before, metal oxide surface groups play an important role in the coordination of HMR suitable for lignan HMR on the Au particle size of Au/Al<sub>2</sub>O<sub>3</sub>. This step is considered to be essential for the HMR transformation. Once the molecule is in the right position, the dehydrogenation proceeds rapidly, enhanced by the presence of activated oxygen.

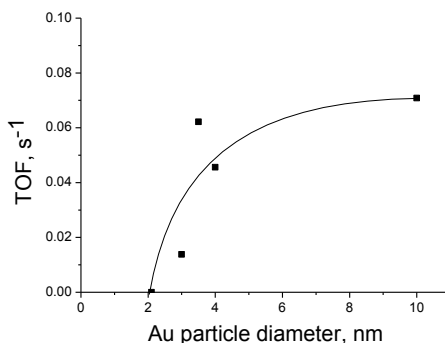


**Figure 15.** The dependence of TOF on the Au particle size in the selective oxidation of HMR on the Au particle size (Au/Al<sub>2</sub>O<sub>3</sub> catalyst).

## 3.3.3.6. Reaction mechanism

The reaction of HMR transformation to oxoMAT is, in fact, a selective oxidation of a secondary alcohol to the corresponding ketone. However, the description of the reaction mechanism is challenging due to different reactivity of HMR diastereomers. The

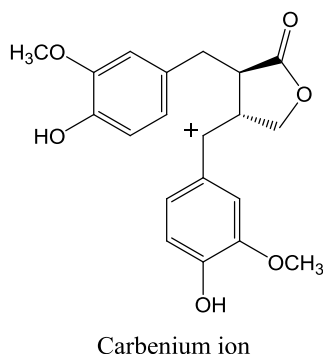


**Figure 16.** HMR 1 and HMR 2 epimerization intermediate

epimerization occurs through the transfer of one proton from the acidic support surface to the alcohol hydroxyl group of both, HMR 1 and HMR 2, resulting in the water molecule release, which leaves the same carbenium ion species on the catalytic surface, irrespectively of the starting HMR epimer (Figure 16). This carbenium species can be easily rehydrated and deprotonated either to HMR 1 or HMR 2.

It was already mentioned, that the lignan HMR could be transformed to oxoMAT in both, anaerobic and aerobic conditions. However, the reaction rate in the presence of oxygen is ca. five times higher, than in its absence. Thus, the HMR transformation over Au includes dehydrogenation steps, while the presence of oxygen

enhances the oxoMAT synthesis.

The difference in the reaction mechanism was investigated by quantum chemical calculations carried out at Dipartimento di Chimica “S. Cannizzaro”, Università degli Studi di Palermo. All the calculations were performed using the Gaussian 03 package. The hybrid Becke’s three parameters exchange-correlation functional B3LYP was used throughout. Los Alamos LANL2 pseudopotential and the corresponding valence basis set were used for Au atoms, while the 6-31G(d,p) basis set was employed for O, C and H atoms. Such a level of the theory was proven to provide reliable structural findings for gold clusters. The starting structure for Au<sub>28</sub> cluster was obtained using a fragment extracted from one Au fcc bulk structure (space group Fm3m,  $a = 4.0782 \text{ \AA}$ ). It was subjected to full geometry optimization. More details on theoretical calculations can be found in ref. [XI].

Since oxoMAT was not formed over pure alumina, the catalytic activity of Au catalysts in the HMR dehydration to oxoMAT can be straightforwardly associated to the presence of gold particles. The results of the calculations confirmed that the HMR transformation over gold includes the dehydrogenation route, not requiring the presence of oxygen.

The state of the activated oxygen on the surface of Au particles is still a matter of debate. There are many studies confirming the involvement of oxygen in the formation of two kinds of surface species, superoxo or peroxy as well as atomic oxygen, active in oxidation. In any case, the participation of activated oxygen in proton removal is agreed and described elsewhere [106]. In the present work, only the activation of oxygen by the Au cluster was considered and dissociative chemisorption, which would certainly require an energy barrier, was not taken into account. The relaxed geometry of the O<sub>2</sub>/Au<sub>28</sub> aggregate has an O<sub>2</sub> molecule in the bridge position: this is the structure, which was used throughout calculations. The optimized geometries of HMR 1 and HMR 2 diastereoisomers interacting with O<sub>2</sub>/Au<sub>28</sub>

system were obtained. In fact, HMR 2 is ca. 0.7 kJ/mol more stable than HMR 1. Moreover, geometrical and electronic parameters pointed out a pronounced structural difference (Figure 17).

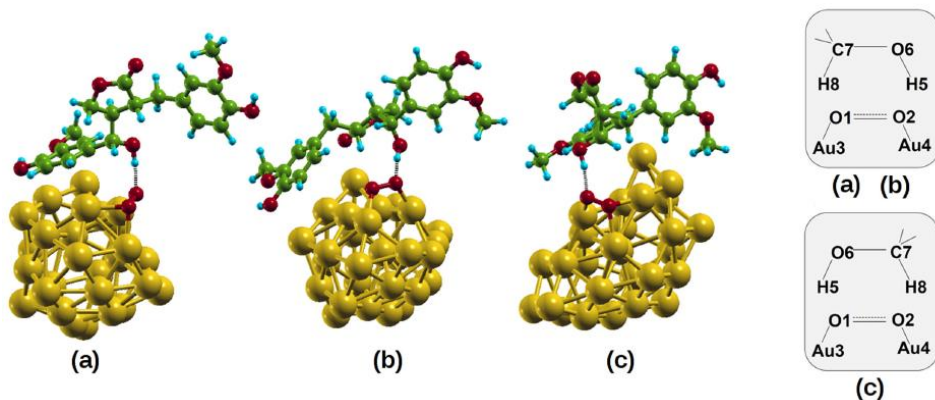


**Figure 17.** Optimized geometries of the HMR epimers on O<sub>2</sub>/Au<sub>28</sub>: (a) and (b) systems represent the most stable HMR 2 (SRR-HMR) and HMR 1 (RRR-HMR) interacting conformer, respectively; (c) is another HMR 1 (RRR-HMR) interacting conformer, which is ca. 8 kJ/mol less stable with respect of (b). The insets on the right report the numbering characterizing the (a) and (b) (top) and (c) systems (bottom).

One of the differences is the O2-H5 distance, which is considerably shorter in the HMR 2+O<sub>2</sub>/Au<sub>28</sub> (1.686 Å) than in the HMR 1+O<sub>2</sub>/Au<sub>28</sub> aggregate (1.747 Å). In brief, the most stable conformation of HMR 2 has the right geometry to interact efficiently with the activated oxygen molecule adsorbed on the gold cluster, while the HMR 1 molecule has presumably to adopt a low population conformation. Even when HMR 1 interacts with the right geometry, small steric effects give rise to an energy barrier for the first hydrogen migration which is ca. 30 kJ/mol higher than the one calculated for the corresponding step in the case of HMR 2 (SRR-HMR) diastereomer. Therefore, theoretical calculations on the dehydrogenation mechanism were presented for the case of more reactive HMR 2 epimer as a model.

The whole dehydrogenation energetic profile is reported in Figure 18. In the present case, the first phase in the process is characterized by a mechanism, in which the O<sub>2</sub> molecule approaches the reactant giving favorable specific interactions and the orientation to promote the C-H hydrogen removal and the subsequent facile O-H bond cleavage. This directly produces an oxoMAT molecule and a characteristic surface di-hydroxide system, (OH)<sub>2</sub>/Au<sub>28</sub>. In the second reaction phase, desorption of the oxoMAT molecule was assumed, thus a second SRR-HMR molecule could interact with the two hydroxyl groups on the Au<sub>28</sub> surface. Therefore, also in this case the presence of oxygen, as hydroxyl group, positively affects the C-H8 bond cleavage by adjusting the orientation of the reactant with the help of a hydrogen bond. Final products are constituted by one (H<sub>2</sub>O)<sub>2</sub>/Au<sub>28</sub> moiety and one more molecule of oxoMAT. On the whole, the reaction is highly exothermic, with an overall energy difference between reactants and products of -300 kJ/mol and -173 kJ/mol for the stages leading to the formation of the first and the second oxoMAT molecule, respectively.

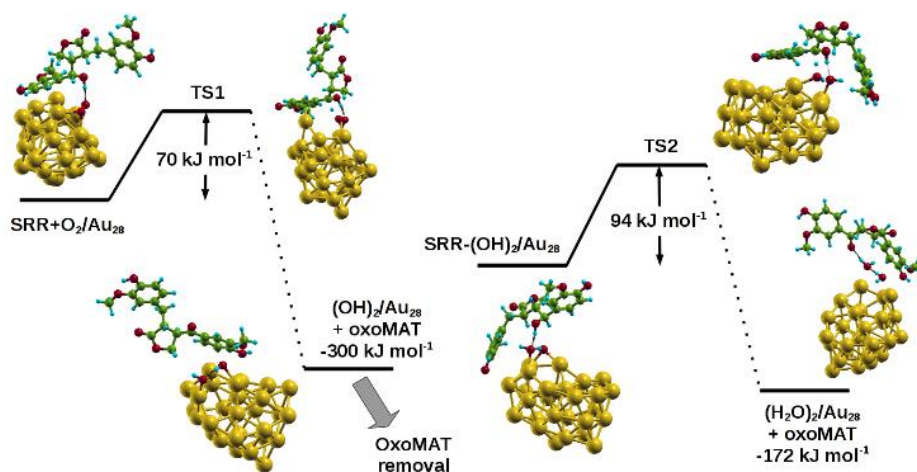


**Figure 18.** SRR-HMR dehydrogenation energetic profile under aerobic conditions.

In anaerobic conditions the dehydrogenation of SRR isomer catalyzed by the  $\text{Au}_{28}$  cluster occurs via a mechanism, which is different from that proposed when activated oxygen is co-adsorbed on the gold surface. The first step, which leaves a first hydrogen atom on the cluster surface, now involves the hydroxyl group deprotonation and is followed by an alcoholate intermediate formation (i.e. the deprotonated SRR-HMR species of Figure 19). In the second step, the C-H hydrogen is also transferred to the gold cluster, with the subsequent oxoMAT formation. Finally, one hydrogen molecule desorbs from the cluster. The activation energies for the first and second step are in the order: 187 and 25 kJ/mol. The whole reaction is slightly endothermic.

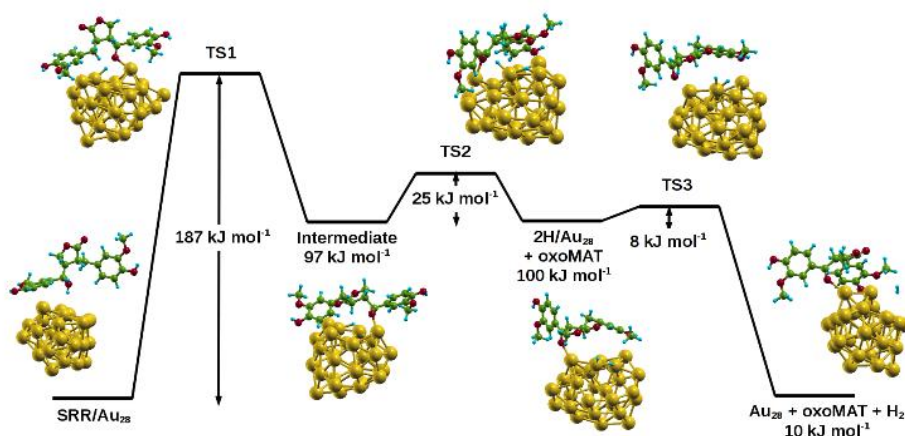


**Figure 19.** HMR 2 (SRR-HMR) dehydrogenation energetic profile under anaerobic conditions.



The results of the calculations underline the role of the activated oxygen in the oxidation of HMR catalyzed by the Au<sub>28</sub> cluster. In the absence of activated oxygen available on the cluster, the dehydrogenation of HMR should occur with much slower kinetics involving a much higher energy barrier. Furthermore, in aerobic conditions, the entire reaction pathway produces two molecules of oxoMAT instead of one. Thus, oxidative dehydrogenation and dehydrogenation are energetically different, the first reaction pathway being preferred.

## 4. Conclusions

---

The growing interest in biomass valorization in recent years has led to an increase of the research on the application of gold catalysts in the transformation of biomass-derived compounds transformations. Gold catalysts have demonstrated an outstanding performance in a number of reactions. This work was focused on the fundamental understanding of the role of nanosized gold catalysts in the transformations of biomass-derived compounds, as well as studying the reaction kinetics, which is important for the future development of biorefinery processes.

Isomerization of linoleic acid over gold catalysts towards biologically active conjugated linoleic acid isomers (CLA) was studied in this work. Gold catalysts were shown to be active in the double bond migration for the first time. The best selectivity towards biologically active *cis*-9,*trans*-11-CLA and *trans*-10,*cis*-12-CLA was achieved by the use of Au/C catalysts.

Selective oxidation of ethanol was performed in gas-phase. Unusual for these conditions, a low-temperature activity of Au/TiO<sub>2</sub> catalysts was observed at 120°C. The formation of an active oxygen species on Au/TiO<sub>2</sub>, responsible for the low temperature oxidation of ethanol over Au/TiO<sub>2</sub> at 80-150°C was proposed. The nature of these oxygen species is not yet clear, although it could be the surface O<sup>-</sup> anion radical, either surface O<sub>2</sub><sup>-</sup> superoxide ions, or hydroperoxo species.

The selective oxidation of L-arabinose was found to be structure sensitive. The procedures for the gold catalyst preparation to achieve different Au particle sizes were studied. The activity of gold catalysts demonstrated a volcano relationship with the Au cluster size.

The selective oxidation of the biomass-derived lignan hydroxymatairesinol (HMR) over gold catalysts was extensively investigated for the first time. Gold catalysts demonstrated a complete selectivity to the desired product – lignan oxomatairesinol (oxoMAT). The highest activity and selectivity to oxoMAT was reached by applying a 2-propanol/water mixture as the solvent, air as the oxidant and Au/Al<sub>2</sub>O<sub>3</sub> as the catalyst. The reaction was found to be structure sensitive. The kinetics and mechanism of the partial oxidation of HMR were studied.

# Notations

---

## Abbreviations

CTO	Crude tall oil
TOFA	Tall oil fatty acid
DTO	Distilled tall oil
CLA	Conjugated linoleic acid
HMR	Hydroxymatairesinol
OxoMAT	Oxomatairesinol
HMR 1 or RRR-HMR	(7R,8R,8'R)-(-)-7- <i>allo</i> -hydroxymatairesinol
HMR 2 or SRR-HMR	(7S,8R,8'R)-(-)-7- <i>allo</i> -hydroxymatairesinol
DIE	Direct ion exchange
DPU	Deposition-precipitation with urea
FTIR	Fourier transmission infrared spectroscopy
CO <sub>2</sub> -TPD	Temperature-programmed desorption of carbon dioxide
TEM	Transmission electron microscopy
XRD	X-ray diffraction
ICP-OES	Inductively coupled plasma optical emission spectroscopy
ICP-AES	Inductively coupled plasma atomic emission spectroscopy
XPS	X-ray photoelectron spectroscopy
TPO	Temperature-programmed oxidation
DSC-TGA	Thermogravimetric analysis with differential scanning calorimetry

# References

- [1] Report of the United Nations Conference on Environment and Development, Rio de Janeiro, June 3-14, 1992, <http://www.un.org/esa/sustdev>.
- [2] Technology Vision 2020, The US Chemical Industry, 1996.  
<http://www.ccrhq.org/vision/index.html>.
- [3] CEFIC, [www.cefic.be](http://www.cefic.be).
- [4] P. Mäki-Arvela, B. Holmbom, T. Salmi, D. Yu. Murzin, *Catal. Rev.* 49 (2007) 197.
- [5] A. Corma, S. Iborra, A. Velty, *Chem. Rev.* 207 (2007) 2411.
- [6] G. Budroni, A. Corma, *J. Catal.* 257 (2008) 403.
- [7] J. N. Chheda, J.A. Dumesic, *Catal. Today*, 123 (2007) 59.
- [8] D. Yu. Murzin, I.L. Simakova, *Catal. Ind.* (in Russian), 2011, (3), 8-40. English translation: 2011, 3, 218-249.
- [9] B.T. Kusema, C. Xu, P. Mäki-Arvela, S. Willför, B. Holmbom, T. Salmi, D. Yu. Murzin, *Int. J. Chem. React. Eng.* 8 (2010) A44: 1.
- [10] J. N. Chheda, G.W. Huber, J.A. Dumesic, *Angew. Chem. Int. Ed.* 46 (2007) 7164.
- [11] N. Sarkar, S. K. Ghosh, S. Bannerjee, K. Aikat, *Renewable Energy* 37 (2012) 19.
- [12] N. Yoneda, S. Kusano, M. Yasui, P. Pujado, S. Wilcher, *Appl. Catal. A* 221 (2001) 253.
- [13] R. Sakamuri, Esters, *Organic in Kirk-Othmer Encyclopedia of Chemical Technology*, online version on Wiley InterScience. DOI: 10.1002/0471238961.05192005200121.a01.pub2.
- [14] C.H. Christensen, B. Jørgensen, J. Rass-Hansen, K. Egeblad, R. Madsen, S.K. Klitgaard, S.M. Hansen, M.R. Hansen, H.C. Andersen, A. Riisager, *Angew. Chem. Int. Ed.* 45 (2006) 4648.
- [15] B. Jørgensen, S.E. Christiansen, M.L.D. Thomsen, C.H. Christensen, *J. Catal.* 251 (2007) 332.
- [16] G. Centi, F. Cavani, F. Trifiro, *Selective Oxidation by Heterogeneous Catalysis*, Kluwer Academic/Plenum Publishers, New York, 2001.
- [17] T. Mallat, A. Baiker, *Chem. Rev.*, 104 (2004) 3037-3058.
- [18] B. Jørgensen, S. B. Kristensen, A. J. Kunov-Kruse, R. Fehrmann, C. H. Christensen, A. Riisager, *Top Catal.*, 52 (2009) 253–257.
- [19] L.-H. Norlin, *Ullmann's Encyclopedia of Industrial Chemistry*, 6th edn.; Wiley-VCH: Weinheim; Vol. 35, 2003, 451-464.
- [20] Y. L. Ha, N. K. Grimm, M. W. Pariza, *Carcinogenesis* 8 (1987) 1881.
- [21] L. D. Whingham, C. A. Watras, D. A. Scholler, *Am. J. Clin. Nutr.* 85 (2007) 1203.
- [22] S. F. Chin, W. Liu, M. Storkson, Y. L. Ha, M. W. Pariza, *J. Food Compos. Anal.* 5 (1992) 185.
- [23] L. D. Whingham, M. E. Cook, R. L. Atkinson, *Pharmacol. Res.* 42 (2000) 503.
- [24] V. Mougios, A. Matsakas, A. Petridou, S. Ring, A. Sagredos, A. Melissopoulou, N. Tsigilis, M. Nikolaidis, *J. Nutr. Biochem.* 12 (2001) 585.
- [25] M. J. T. Reaney, Y. D. Liu, N. D. Westcott, *Commercial Production of Conjugated Linoleic Acid*. In *Advances in Conjugated Linoleic Acid Research*, Vol. 1, M. P. Yurawecs, M. M. Massoba, J. K. G. Kramer, M. W. Pariza, G. J. Nelson (editors). Champaign, IL, AOCS Press (1999) 39-54.
- [26] P. R. O'Quinn, J. L. Nelssen, R. D. Goodband, M. D. Tokach, *Animal Health Research Reviews*, 1 (2000) 35.
- [27] W. DeJarlais, L. Gast, *Journal of the American Oil Chemists' Society* 48 (1971) 21.
- [28] E. Frankel, *Journal of the American Oil Chemists' Society* 47 (1970) 11.
- [29] A. Bernas, N. Kumar, P. Mäki-Arvela, E. Laine, B. Holmbom, T. Salmi, D.Yu. Murzin, *Chem. Commun.* 10 (2002) 1142.
- [30] A. Philippaerts, S. Goossens, W. Vermandel, M. Tromp, S. Turner, J. Geboers, G. Van Tendeloo, P. A. Jacobs, B. F. Sels, *ChemSusChem* 4 (2011) 757.

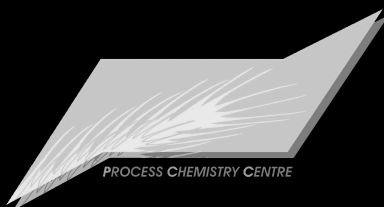
- [31] R. Ekman, *Holzforschung* 30 (1976) 79.
- [32] S. Willför, P. Eklund, R. Sjöholm, M. Reunanen, R. Sillanpää, S. von Schoultz, J. Hemming, L. Nisula, B. Holmbom, *Holzforschung* 59 (2005) 413.
- [33] P. C. Eklund, S. Willför, A. Smeds, B. R. Holmbom, R. E. Sjöholm, *J. Nat. Prod.* 67 (2004) 927.
- [34] S. Willför, J. Hemming, M. Reunanen, C. Eckerman, B. Holmbom, *Holzforschung* 57 (2003) 27.
- [35] H. Adlercreutz, *Phytoestrogens and Human Health*, In: *Reproductive and Developmental Toxicology* (edited by Korach, K.), Marcel&Dekker, NY, 1998, pp. 299-371.
- [36] S. M. Willför, M. O. Ahotupa, J. E. Hemming, M. H. T. Reunanen, P. C. Eklund, R. E. Sjöholm, C. S. E. Eckerman, S. P. Pohjamo, B. R. Holmbom, *J. Agr. Food Chem.* 51 (2003) 7600.
- [37] S. Yamaguchi, T. Sugahara, Y. Nakashima, A. Okada, K. Akiyama, T. Kishida, M. Maruyama, T. Masuda, *Biosci. Biotechnol. Biochem.* 70 (2006) 1934.
- [38] P. C. Eklund, O. K. Långvik, J. P. Wärnå, T. O. Salmi, S. M. Willför, R. E. Sjöholm *Org. Biomol. Chem.* 3 (2005) 3336.
- [39] H. Korte, M. Unkila, M. Hiilovaara-Teijo, V.-M. Lehtola, M. Ahotupa, Patent WO/2004/000304 A1 (2003).
- [40] T. Ahlnäs, Patent WO 2008/020112 A1 (2008).
- [41] F. Kawamura, M. Miyachi, S. Kaway, *J. Wood Sci.* 44 (1998) 47.
- [42] P. Eklund, A. Lindholm, J.-P. Mikkola, A. Smeds, R. Lehtilä, R. Sjöholm, *Org. Lett.* 5 (2003) 491.
- [43] H. Markus, A. J. Plomp, T. Sandberg, V. Nieminen, J. H. Bitter, D. Yu. Murzin, *J. Mol. Catal. A.* 274 (2007) 42.
- [44] M. Haruta, T. Kobayashi, H. Sano, N. Yamada, *Chem. Lett.* 2 (1987) 405.
- [45] A. Abad, P. Conception, A. Corma, H. Garcia, *Angew. Chem. Int. Ed.* 44 (2005) 4066.
- [46] A. Corma, M.E. Domine, *Chem. Commun.* 32 (2005) 4042.
- [47] US Patent 374 2079 to Mobil Oil Corp. (1973); *Chem. Abs.* 79 (1973) 92807.
- [48] M. D. Hughes, Y.-J. Xu, P. Jenkins, P. McMorn, P. Landon, D. I. Enache, A. F. Carley, G. A. Attard, G. J. Hutchings, F. King, E. H. Stitt, P. Johnstone, K. Griffin, C. J. Kiely, *Nature* 437 (2005) 1132.
- [49] R. Zhao, D. Ji, G. Lv, G. Qian, L. Yan, X.-L. Wang, J. Suo, *Catal. Lett.* 97 (2004) 115.
- [50] M. Comotti, C. Della Pina, R. Matarrese, M. Rossi, *Angew. Chem., Int. Ed.*, 43 (2004) 5812.
- [51] F. Porta, L. Prati, *J. Catal.*, 224 (2004) 397.
- [52] S. Carrettin, P. McMorn, P. Johnstone, K. Griffin, G.J. Hutchings, *Chem. Commun.* (2002) 697.
- [53] Z. Hao, L. An, H. Wang, T. Hu, *React. Kinet. Catal. Lett.* 70 (2000) 153.
- [54] G. C. Bond, D. T. Thompson, *Catal. Rev. Sci. Eng.* 41 (1999) 319.
- [55] N. Lopez, T. V. P. Janssens, B. S. Claussen, Y. Xu, M. Mavrikakis, T. Bligaard, J. K. Nørskov, *J. Catal.* 223 (2004) 232.
- [56] B. Hvolbæk, T. V. W. Janssens, B. S. Claussen, H. Falsig, C. H. Christensen, J. K. Nørskov, *Nanotoday* 2 (2007) 14.
- [57] F. Boccuzzi, A. Chiorino, S. Tsubota, M. Haruta, *J. Phys. Chem. B*, 100 (1996) 3625.
- [58] S. Miscino, S., Scire, C. Crisafulli, A. M. Visco, S. Galvagno, *Catal. Lett.* 44 (1997) 273.
- [59] A. Sanchez, S. Abbet, U. Heiz, W.-D. Schneider, H. Hakkinen, R. N. Barnett, U. Landman, *J. Phys. Chem. A* 103 (1999) 9573.
- [60] Y. Xu, M. Mavrikakis, *J. Phys. Chem. B* 107 (2003) 690.
- [61] B. E. Salisbury, W. T. Wallance, R. L. Whetten, *Chem. Phys.* 262 (2000) 131.
- [62] M. Stratakis, H. Garcia, *Chem. Rev.* 2012 (dx.doi.org/10.1021/cr3000785).
- [63] G. C. Bond, P. A. Sermon, G. Webb, D. A. Buchanan, P. B. Wells, *J. Chem. Soc. Chem. Commun.* (1973) 444.

- [64] P. Claus, *Appl. Catal. A* 291 (2005) 222.
- [65] A. Corma, P. Serna, *Science* 313 (2006) 5785.
- [66] A. Corma, P. Concepcion, P. Serna, *Angew. Chem. Int. Ed.* 46 (2007) 7266.
- [67] H. Markus, P. Mäki-Arvela, N. Kumar, N. V. Kul'kova, P. Eklund, R. Sjöholm, B. Holmbom, T. Salmi and D. Yu. Murzin, *Catal. Lett.* 103 (2005) 125.
- [68] S. Ivanova, V. Pitchon, Y. Zimmermann, C. Petit, *Appl. Catal. A* 298 (2006) 57.
- [69] E.V. Murzina, A.V. Tokarev, K. Kordás, H. Karhu, J.-P. Mikkola, D. Yu. Murzin, *Catal. Today* 131 (2008) 385.
- [70] F. Porta, L. Prati, M. Rossi, S. Coluccia, G. Martra, *Catal. Today* 61 (2000) 165.
- [71] V. V. Kriventsov, I. L. Simakova, A. Simakov, E. Smolentseva, F. Castillon, M. Estrada, E. Vargas, E. P. Yakimchuk, D. P. Ivanov, D. G. Aksenov, D. V. Andreev, B. N. Novgorodov, D. I. Kochubey, S. Fuentes, *Nucl. Instrum. Method. Phys. Res. A* 603 (2009) 185.
- [72] G. Pérez, S. Fuentes, V. Petranovskii, A. Simakov, *Catal. Lett.* 110 (2006) 53.
- [73] M. Zaki, M. Hasan, F. A. Al-Sagheer, L. Pasupulety, *Colloids Surf. A* 190 (2001) 261.
- [74] A. Bernas, N. Kumar, P. Mäki-Arvela, N.V. Kul'kova, B. Holmbom, T. Salmi, D. Yu. Murzin, *Appl. Catal. A* 245 (2003) 257.
- [75] T. Mallat, A. Baiker, *Catal. Today* 19 (1994) 247–284.
- [76] B. T. Kusema, B. C. Campo, P. Mäki-Arvela, T. Salmi, D. Yu. Murzin, *Appl. Catal. A* 386 (2010) 101.
- [77] S. Ardizzzone, C. L. Bianchi, B. Vercelli, *Colloids Surf. A* 144 (1-3) (1998) 9.
- [78] P. A. Simonov, V. A. Likholobov, in: A. Wieckowski, E. R. Savinova, C. G. Vayenas (Eds.), *Catalysis and Electrocatalysis at Nanoparticle Surfaces*, Marcel Dekker, New York, 2003, p. 409.
- [79] E. Selli, L. Forni, *Microporous Mesoporous Mater.* 31 (1999) 129.
- [80] A. Aho, N. Kumar, K. Eränen, M. Huppa, T. Salmi, D. Yu. Murzin, *Proceedings of 4th International FEZA Conference*, A. Gedeon, P. Massiani, F. Babonneau (Eds.), 2008, 1069.
- [81] P. Claus, A. Brüchler, C. Mohr and H. Hofmeister, *J. Am. Chem. Soc.*, 122 (11) (2000) 430.
- [82] A. Sanchez, S. Abbet, U. Heiz, W.-D. Schneider, H. Häkkinen, R. N. Barnett and U. Landman, *J. Phys. Chem. A*, 103 (1999) 9573.
- [83] J. Radnik, C. Mohr, P. Claus, *Phys. Chem. Chem. Phys.* 5 (2003) 172.
- [84] G. C. Bond, in: B. Imelik, C. Naccache, G. Courier, H. Praliaud, P. Meriaudeau, P. Gallezot, G. A. Martin, J. C. Vedrine *Metal-Support and Metal Additive Effects in Catalysis*, ed., Elsevier, Amsterdam, 1982, ch. 1.
- [85] J. F. Moulder, W. F. Stickle, P. E. Sobol, K. D. Bomben *Handbook of X-ray Photoelectron Spectroscopy*, Eden Prairie: Perkin-Elment // Corporation Physical Electronics Division. – 1992, p.179.
- [86] A. M. Visco, F. Neri, G. Neri, A. Donato, C. Milone, S. Galvagno, *Phys. Chem. Chem. Phys.* 1 (1999) 2869.
- [87] F.-W. Chang, H.-Y. Yu, L. S. Roselin, H.-C. Yang, T.-C. Ou, *Appl. Catal. A: Gen.* 302 (2006) 157.
- [88] A. Corma, H. Garcia, *Chem. Soc. Rev.* 37 (2008) 2096.
- [89] E. Smolentseva, A. Simakov, S. Beloshapkin, M. Estrada, E. Vargas, V. Sobolev, R. Kenzhin, S. Fuentes, *Appl. Catal. B: Environ* 115-116 (2012) 117.
- [90] T. Salama, T. Shido, R. Ohnishi, M. J. Ichikawa, *J. Phys Chem.* 100 (1996) 3688.
- [91] V.W.-W. Yam, C.-L. Chan, C.-K. Li, K. M.-C. Wong, *Coord. Chem. Rev.* 216-217 (2001) 173.
- [92] W. Chen, J. Zhang, W. Cai, *Scr. Mater.* 48 (2003) 1061.
- [93] I. Tuzovskaya, N. Bogdanchikova, A. Simakov, V. Gurin, A. Pestryakov, M. Avalos, M. Farias, *Chem. Phys.* 338 (2007) 23.

- 
- [94] E. Smolentseva, A. Simakov, S. Beloshapkin, M. Estrada, E. Vargas, V. Sobolev, R. Kenzhin, S. Fuentes, *Appl. Catal. B: Environ* 115-116 (2012) 117.
- [95] M. L. Poutsma, *Am. Chem. Soc. Monogr.*, 171 (1971) 431.
- [96] D. Mukesh, C. Narasimhan, V. M. Deshpande, K. Ramnarayan, *Ind. Eng. Chem. Res.*, 27 (1988) 409.
- [97] C. Della Pina, E. Falletta, L. Prati, M. Rossi, *Chem. Soc. Rev.* 37 (2008) 2077.
- [98] A. Corma, H. Garcia, *Chem. Soc. Rev.* 37 (2008) 2096.
- [99] A. S. K. Hashmi, *Chem. Rev.* 107 (2007) 3180.
- [100] A. S. K. Hashmi, G. J. Hutchings, *Angew. Chem. Int. Ed.* 45 (2006) 7896.
- [101] G. I. Panov, V. I. Sobolev, A. S. Kharitonov, *J. Mol. Catal.* 61 (1990) 85.
- [102] J. F. Montoya, J. Peral, P. Salvador, *ChemPhysChem* 12 (2011) 901.
- [103] Y. Önal, S. Schimpf, P. Claus, *J. Catal.* 223 (2004) 122.
- [104] D. Yu. Murzin, *J. Molec. Catal. A. Chem.*, 315 (2010) 226.
- [105] B. T. Kusema, J.-P. Mikkola, D. Yu. Murzin, *Catal. Sci. Technol.*, 2 (2012) 423.
- [106] Y. Guan, E.J.M. Hensen, *Appl. Catal. A* 361 (2009) 49.
- [107] X. Yang, X. Wang, C. Liang, W. Su, C. Wang, Z. Feng, C. Li, J. Qiu, *Catal. Commun.*, 9 (2008) 2278-2281.
- [108] B. N. Zope, D. D. Hibbitts, M. Neurock, R. J. Davis, *Science* 330 (2010) 74-78.
- [109] B. K. Min, C. M. Friend, *Chem. Rev.* 107 (2007) 2709-2724.
- [110] S. E. Davis, B. N. Zope, R. J. Davis, *Green Chem.*, DOI: 10.1039/c1gc16074e.
- [111] D. Yu. Murzin, N. V. Kul'kova, *Catal. Today* 24 (1995) 35.







**ISBN 978-952-12-2793-6**

**PAINOSALAMA OY  
TURKU, FINLAND 2012**